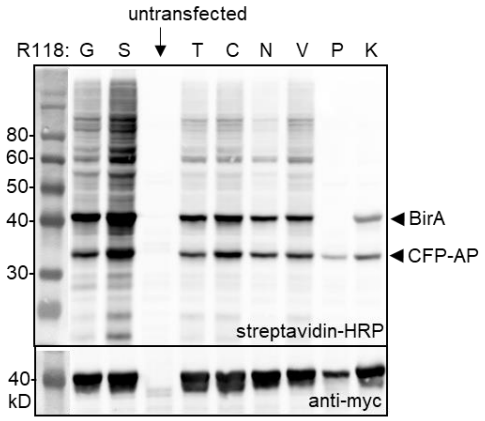

Supplementary Figure 1. Testing R118 mutations in *E. coli* biotin ligase (BirA). The indicated mutants were transiently expressed as NES (nuclear export signal) fusions in the HEK cytosol. All samples were co-transfected with AP-CFP (biotin ligase acceptor peptide (AP) fused to cyan fluorescent protein), a known peptide substrate for wild-type BirA[1]. 50 μM biotin was added to the cells for 18 hours, then whole cell lysates were analyzed by streptavidin-HRP blotting. Ligase expression was detected by anti-myc blotting. Based on these results, we selected BirA-R118S as our template for directed evolution of TurboID. This experiment was performed once, but direct comparison of BirA-R118G to BirA-R118S was performed twice with similar results.

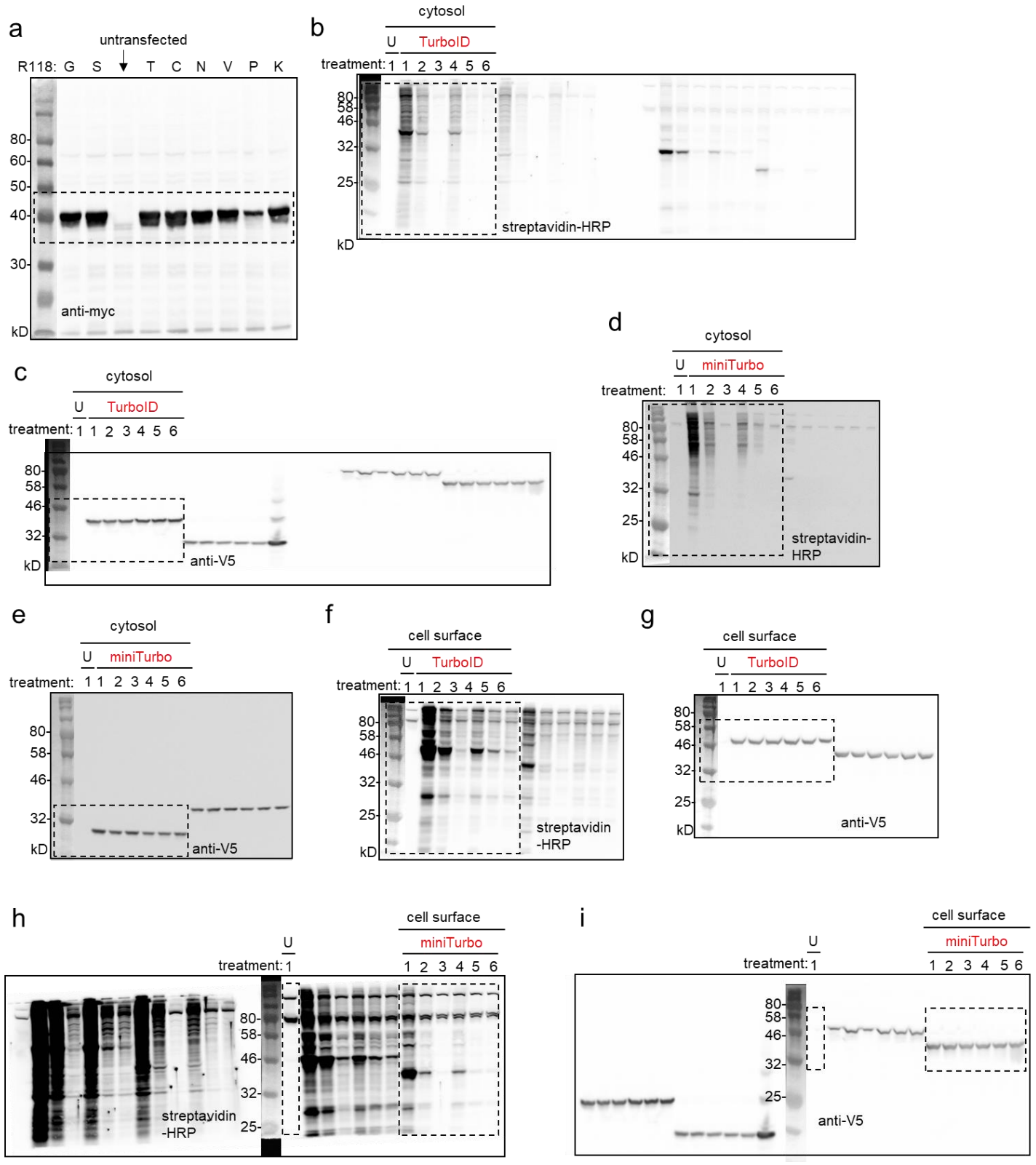

Supplementary Figure 2. Complete gel images for main and supplementary figures. Dotted lines denote regions shown in Figures. Not shown are gels/blots that are already uncropped in main and supplementary figures. (**a**) Supplementary Figure 1 anti-myc blot. (**b**) Supplementary Figure 5a TurboID streptavidin blot. (**c**) Supplementary Figure 5a TurboID anti-V5 blot. (**d**) Supplementary Figure 5a miniTurbo streptavidin blot. (**e**) Supplementary Figure 5a miniTurbo anti-V5 blot. (**f**) Supplementary Figure 5b TurboID streptavidin blot. (**g**) Supplementary Figure 5b TurboID anti-V5 blot. (**h**) Supplementary Figure 5b miniTurbo streptavidin blot. (**i**) Supplementary Figure 5b miniTurbo anti-V5 blot.

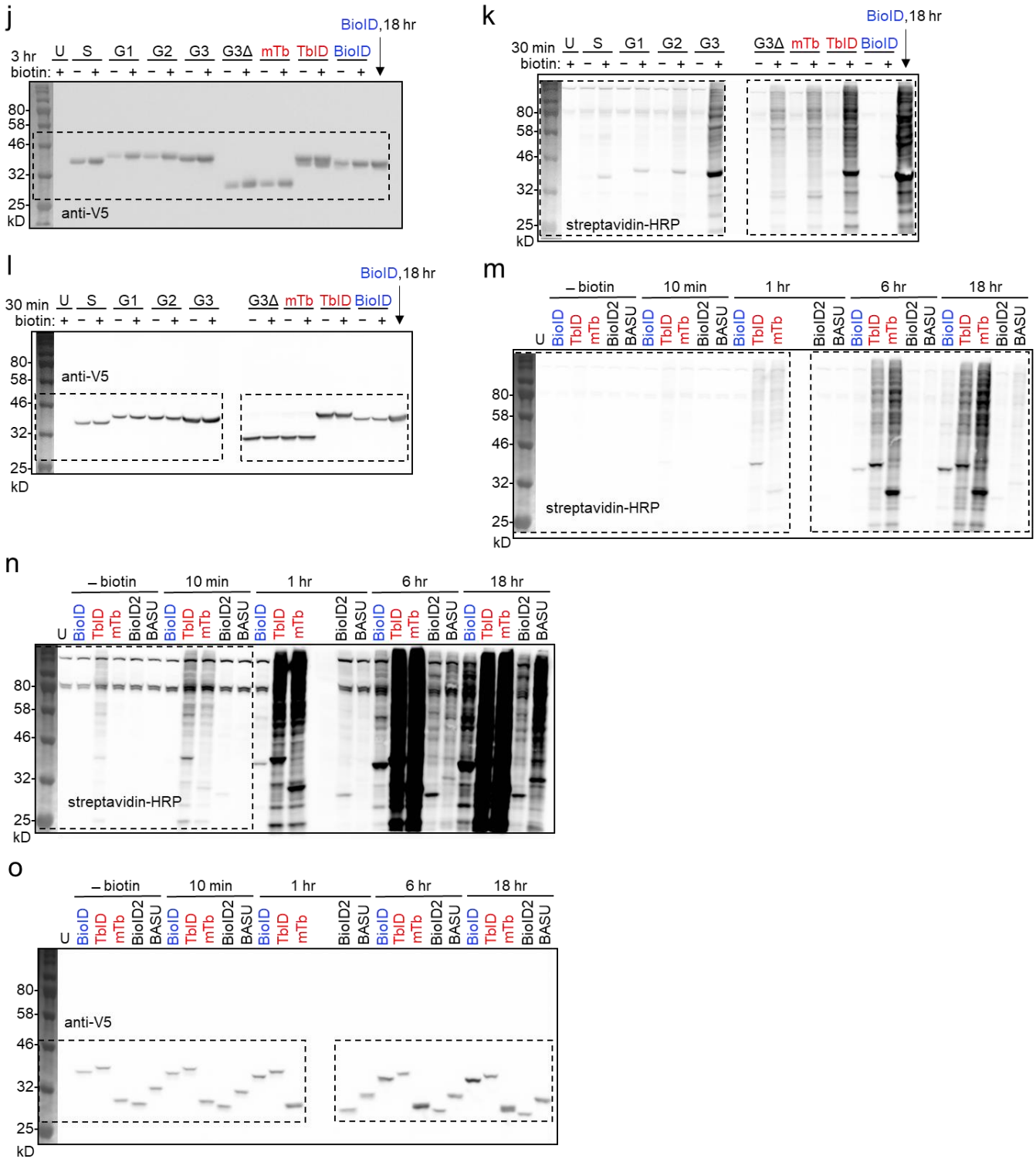

Supplementary Figure 2 (continued). Complete gel images for main and supplementary figures. Dotted lines denote regions shown in Figures. (**j**) Figure 1f anti-V5 blot. (**k**) Supplementary Figure 4b streptavidin blot. (**l**) Supplementary Figure 4b anti-V5 blot. (**m**) Figure 2a streptavidin blot. (**n**) Figure 2a streptavidin blot "longer exposure" inset. (**o**) Figure 2a anti-V5 blot.

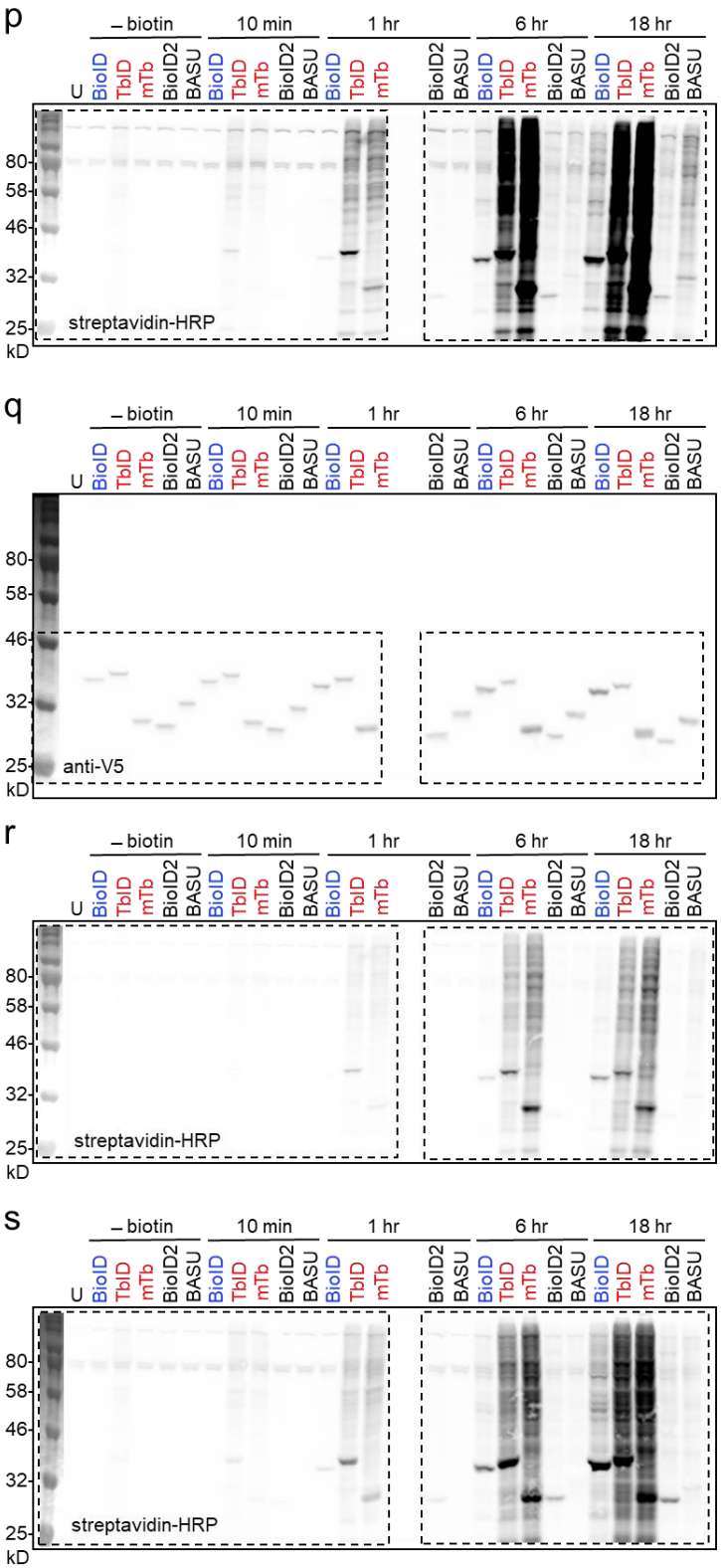

Supplementary Figure 2 (continued). Complete gel images for main and supplementary figures. Dotted lines denote regions shown in Figures. (**p**) Supplementary Figure 6a streptavidin blot. (**q**) Supplementary Figure 6a, b anti-V5 blot. (**r**) Supplementary Figure 6b streptavidin blot. (**s**) Supplementary Figure 6c streptavidin blot.

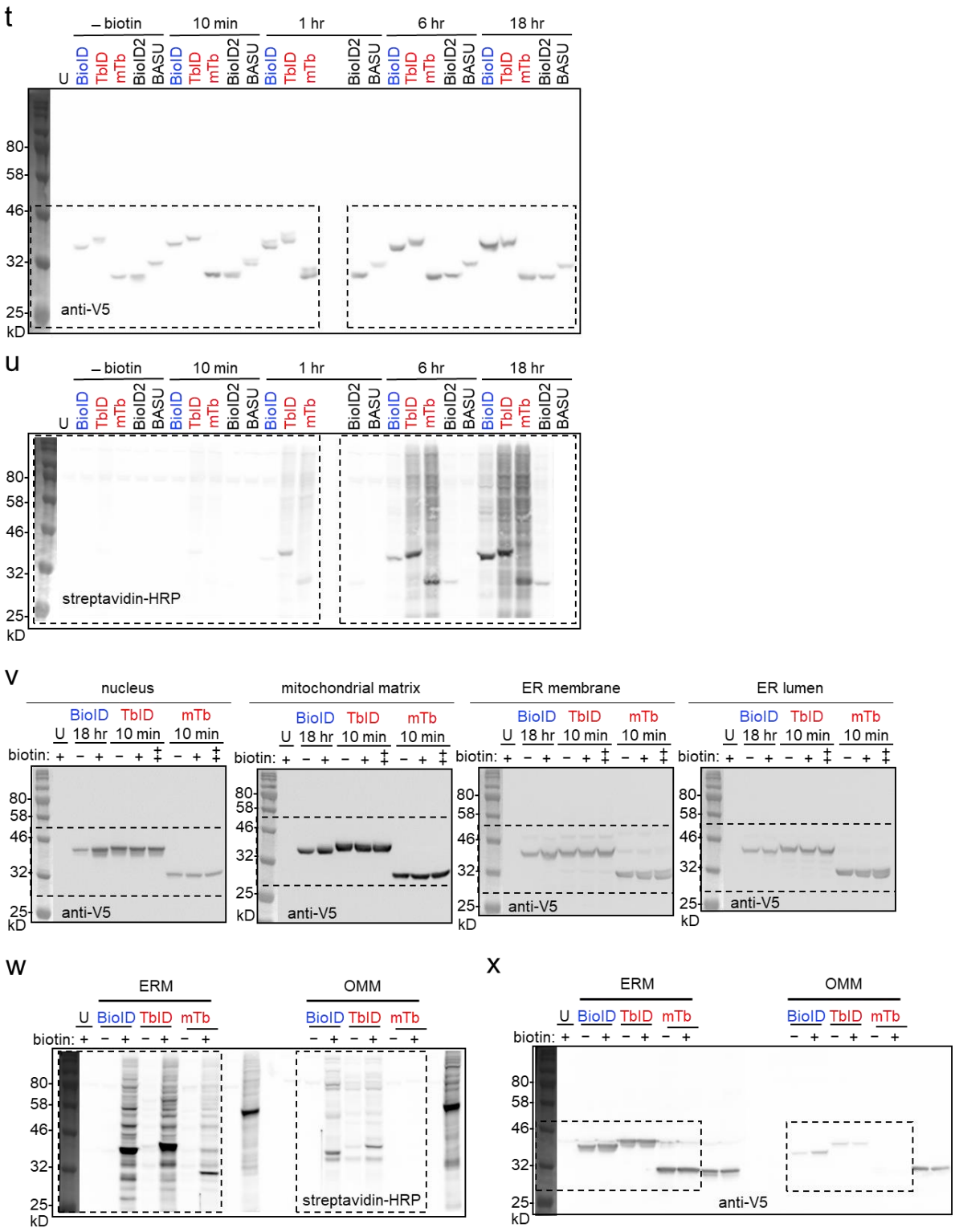

Supplementary Figure 2 (continued). Complete gel images for main and supplementary figures. Dotted lines denote regions shown in Figures. (**t**) Supplementary Figure 6c, d anti-V5 blot. (**u**) Supplementary Figure 6c streptavidin blot. (**v**) Figure 2c anti-v5 blots. (**w**) Supplementary Figure 8b streptavidin blot. (**x**) Supplementary figure 8b anti-V5 blot.

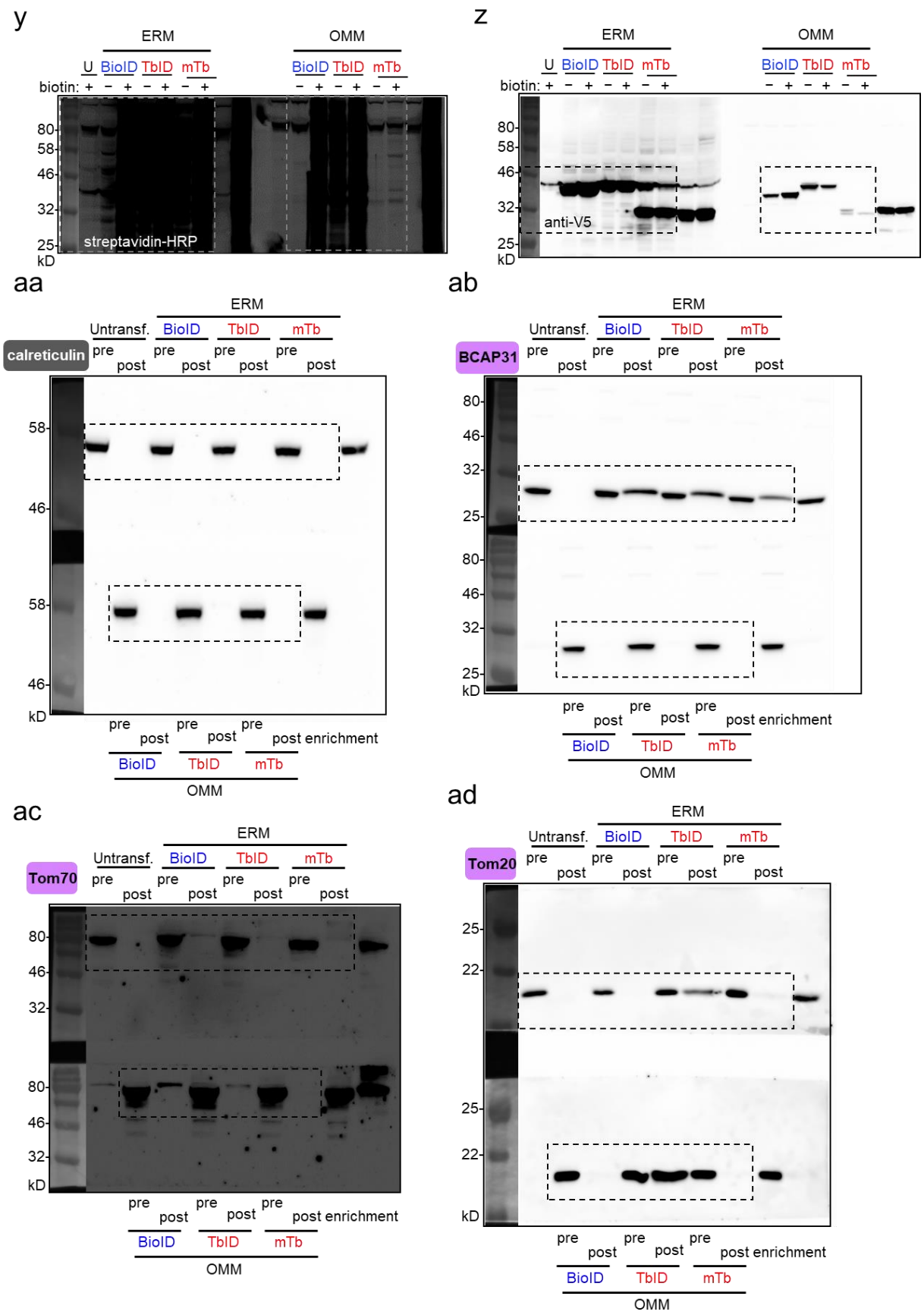

Supplementary Figure 2 (continued). Complete gel images for main and supplementary figures. Dotted lines denote regions shown in Figures. (**y**) Supplementary Figure 8c streptavidin blot. (**z**) Supplementary figure 8c anti-V5 blot. (**aa**) Supplementary Figure 8d anti-calreticulin blot. (**ab**) Supplementary Figure 8d anti-BCAP31 blot. (**ac**) Supplementary Figure 8d anti-Tom70 blot. (**ad**) Supplementary Figure 8d anti-Tom20 blot.

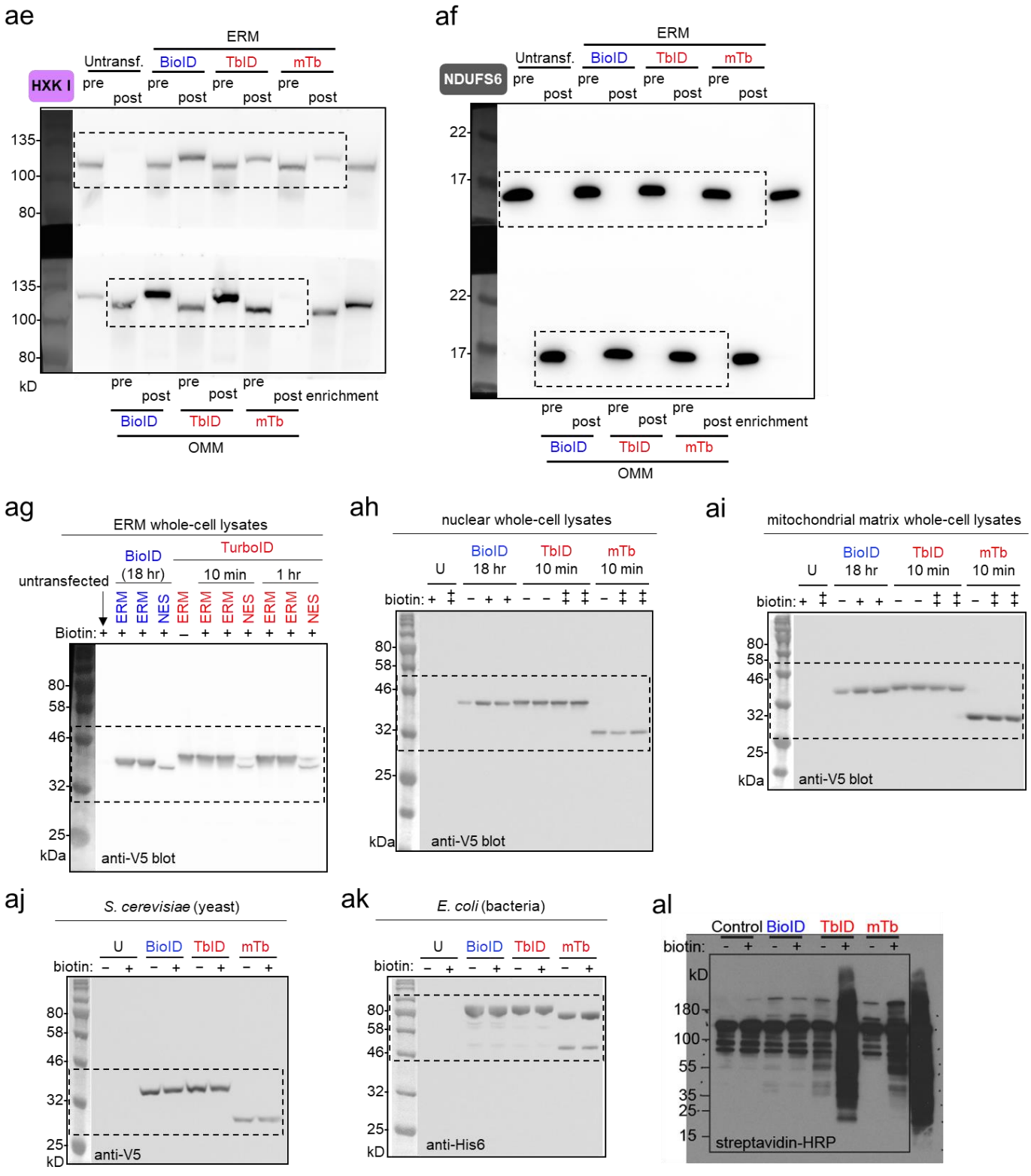

Supplementary Figure 2 (continued). Complete gel images for main and supplementary figures. Dotted lines denote regions shown in Figures. (**ae**) Supplementary Figure 8d anti-HXK I blot. (**af**) Supplementary Figure 8d anti-NDUFS6 blot. (**ag**) Supplementary Figure 9a anti-V5 blot. (**ah**) Supplementary Figure 10b anti-V5 blot. (**ai**) Supplementary Figure 10c anti-V5 blot. (**aj**) Figure 3a anti-V5 blot. (**ak**) Figure 3b anti-His6 blot. (**al**) Figure 3g streptavidin blot.

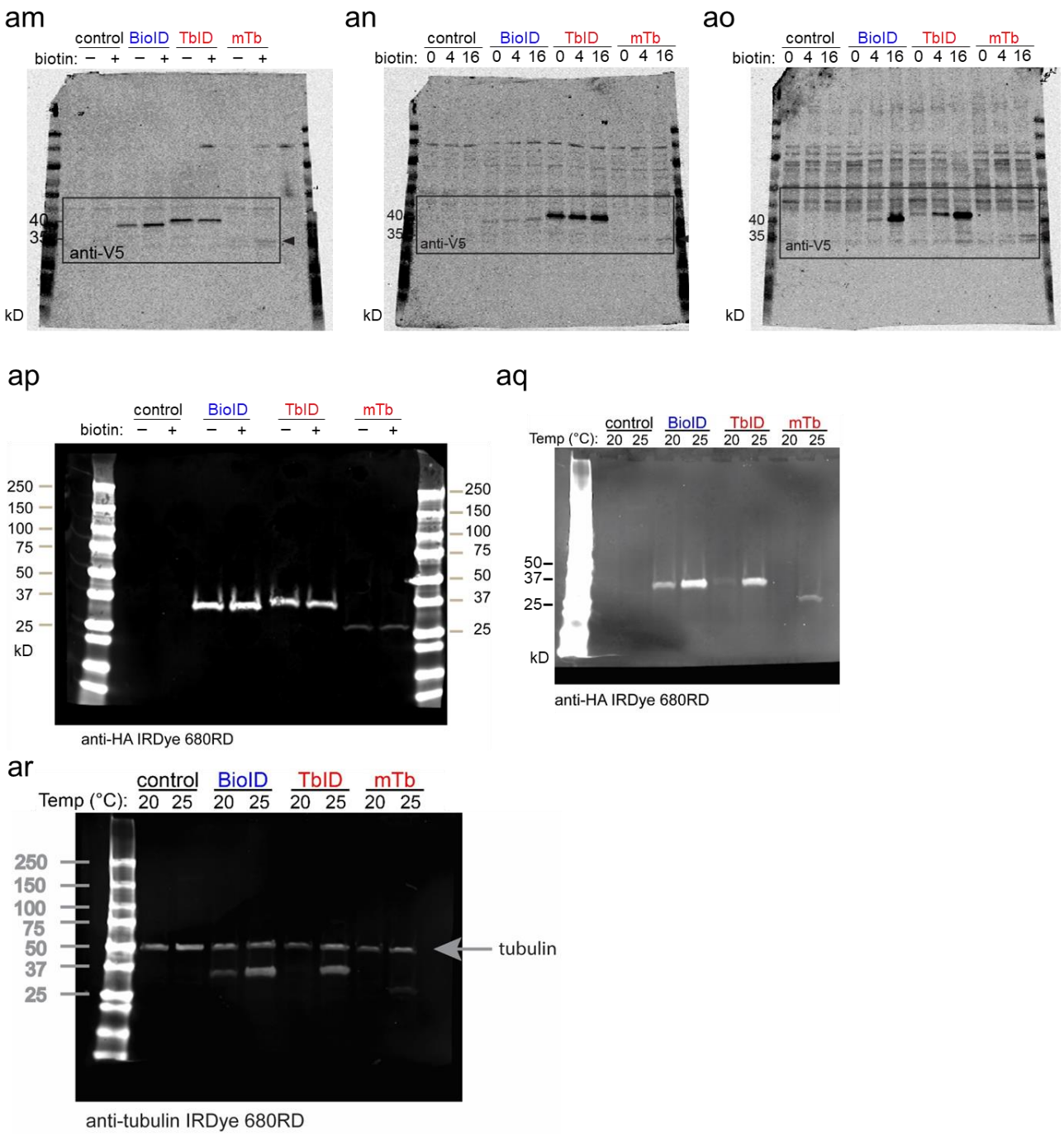

Supplementary Figure 2 (continued). Complete gel images for main and supplementary figures. Dotted lines denote regions shown in Figures. (**am**) Figure 3g anti-V5 blot. (**an**) Supplementary Figure 12b anti-V5 blot. (**ao**) Supplementary Figure 12d anti-V5 blot. (**ap**) Figure 3i anti-HA blot. (**aq**) Supplementary Figure 15g anti-HA blot. (**ar**) Supplementary Figure 15g anti-tubulin blot.

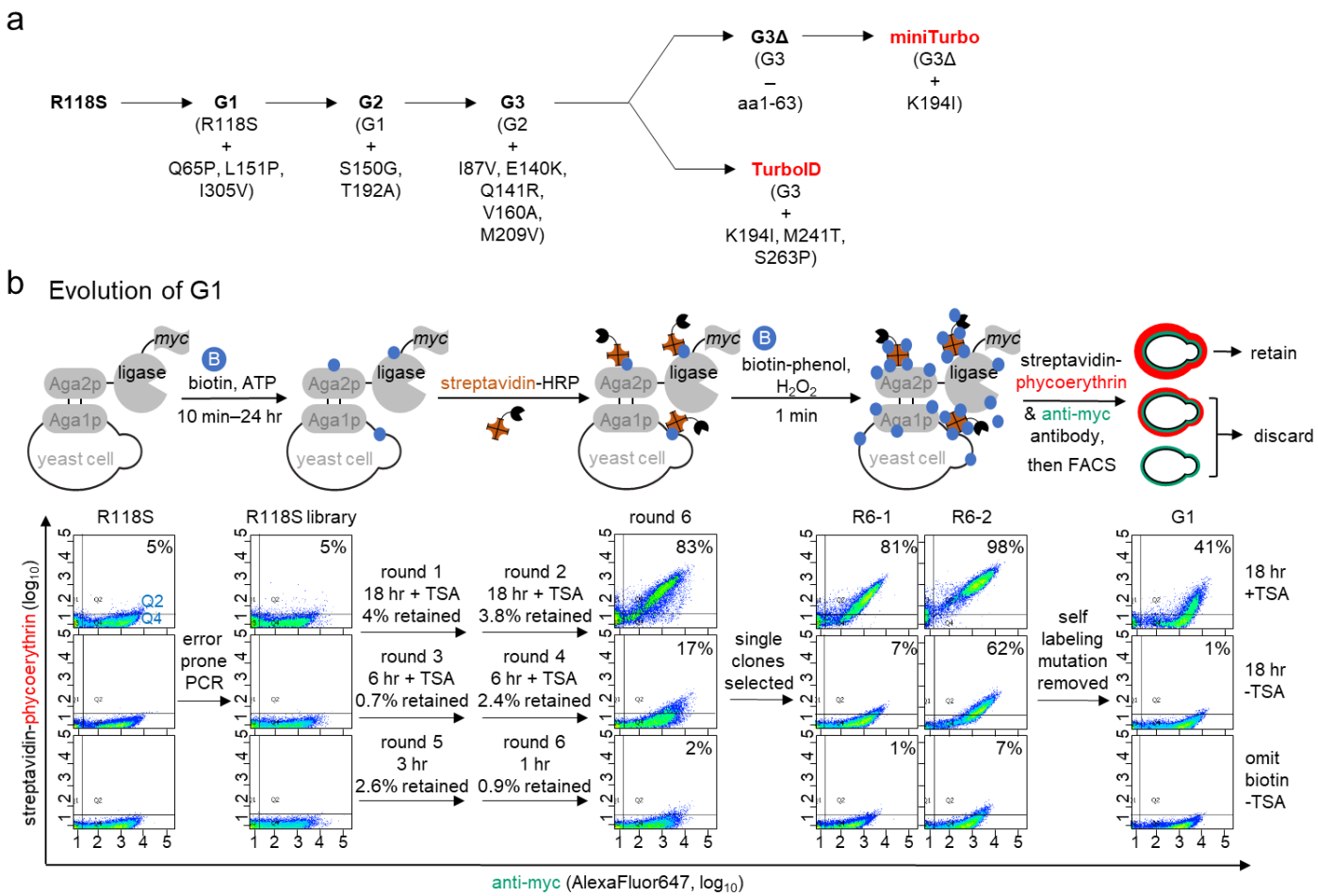

Supplementary Figure 3. Evolution of TurboID and miniTurbo via yeast display. For FACS plots, percentage of cells in upper right quadrant (Q2/(Q2+Q4)) shown in top right of each graph; where no percentage shown, <1%. (**a**) We performed three generations of directed evolution (shown in panels b, c, and d) to produce clone G3 (third generation winning clone). We then branched to two additional generations of evolution to produce miniTurbo (g) and TurboID (h). (**b**) Selection scheme and FACS data for first generation of evolution, to produce clone G1 (first generation winning clone). Here, due to extremely low activity of the starting library, it was necessary to use TSA (tyramide signal amplification[2]) to amplify the biotin signal. Below: FACS data for the indicated yeast samples are shown under three conditions: 18 hours with 50 μM biotin, 1 mM ATP, and 5 mM $MgCl_2$, followed by TSA signal amplification as in (a) (top row); same but without TSA signal amplification (middle row); or no treatment and no amplification (bottom row). Cells were stained with streptavidin-phycoerythrin to detect biotinylation sites (y axis) and anti-myc antibody to quantify ligase expression level (x axis). Above the arrows are given the labeling conditions used in each of the six rounds of selection, and the fraction of cells collected via FACS in each round. This experiment was performed once.

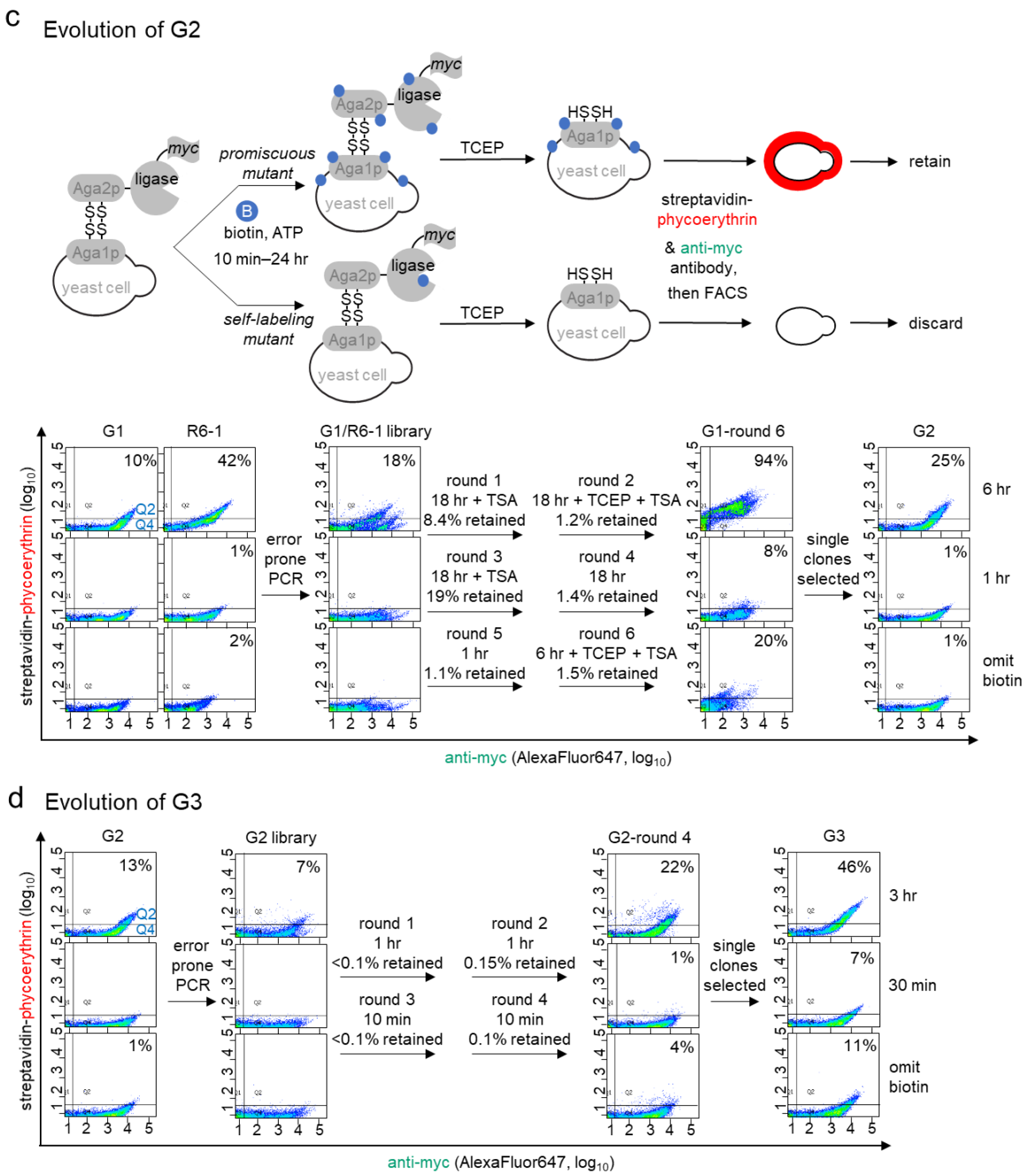

Supplementary Figure 3 (continued). Evolution of TurboID and miniTurbo via yeast display. For FACS plots, percentage of cells in upper right quadrant (Q2/(Q2+Q4)) shown in top right of each graph; where no percentage shown, <1%. (**c**) Selection scheme and FACS data for second generation of evolution, evolving clone G1 into clone G2. Scheme shows how the use of TCEP to reduce the disulfide bonds linking ligase to the yeast surface enables us to separate promiscuous mutants from mutants that merely biotinylate themselves. FACS data and labeling conditions used for each of 6 rounds of selection given below. In some rounds, we again employed TSA to amplify signal. Each of the indicated samples is shown under three different labeling conditions. This experiment was performed once. (**d**) FACS data for third generation of evolution, evolving clone G2 into clone G3. Selection conditions used in rounds 1-4 shown. No TCEP or TSA were used in these rounds. This experiment was performed once.

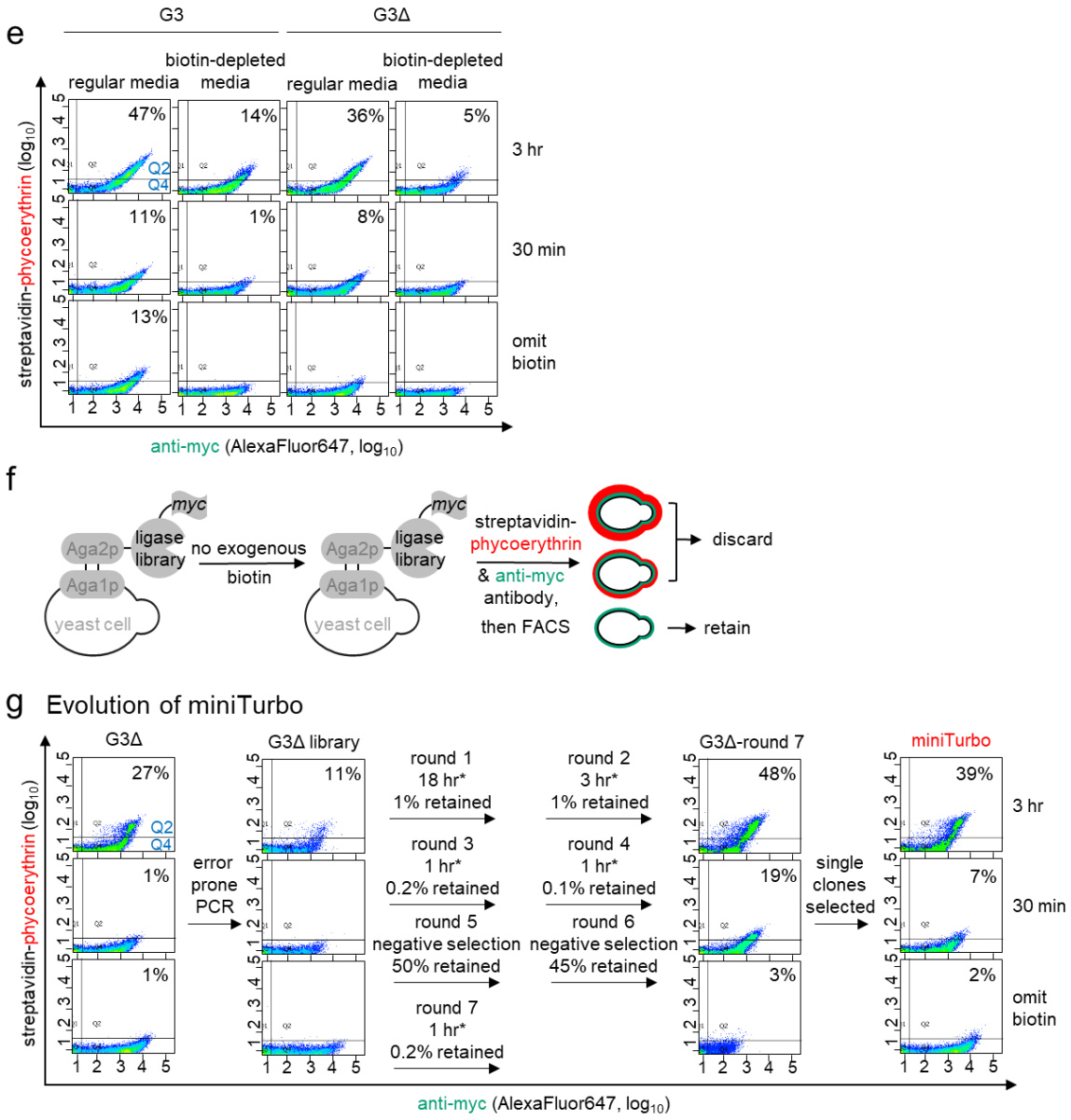

Supplementary Figure 3 (continued). Evolution of TurboID and miniTurbo via yeast display. For FACS plots, percentage of cells in upper right quadrant (Q2/(Q2+Q4)) shown in top right of each graph; where no percentage shown, <1%. (**e**) FACS plots showing that clone G3 gives biotinylation in the absence of exogenous biotin. When G3 yeast are cultured in biotin-depleted media, this signal is no longer detected (second column). Deletion of the N-terminal domain to give G3Δ reduces biotin affinity and consequently biotinylation activity prior to exogenous biotin addition (third and fourth columns). This experiment was performed once. (**f**) Scheme for negative selections employed in the fourth generation of evolution. (**g**) FACS data showing the evolution of miniTurbo from G3Δ. Seven rounds of selection were performed, with rounds 5 and 6 being negative selections as in (f) to remove mutants with high biotin affinity. Asterisks denote selections performed in biotin-depleted media. The three analysis conditions were also performed in biotin-depleted media. This experiment was performed once.

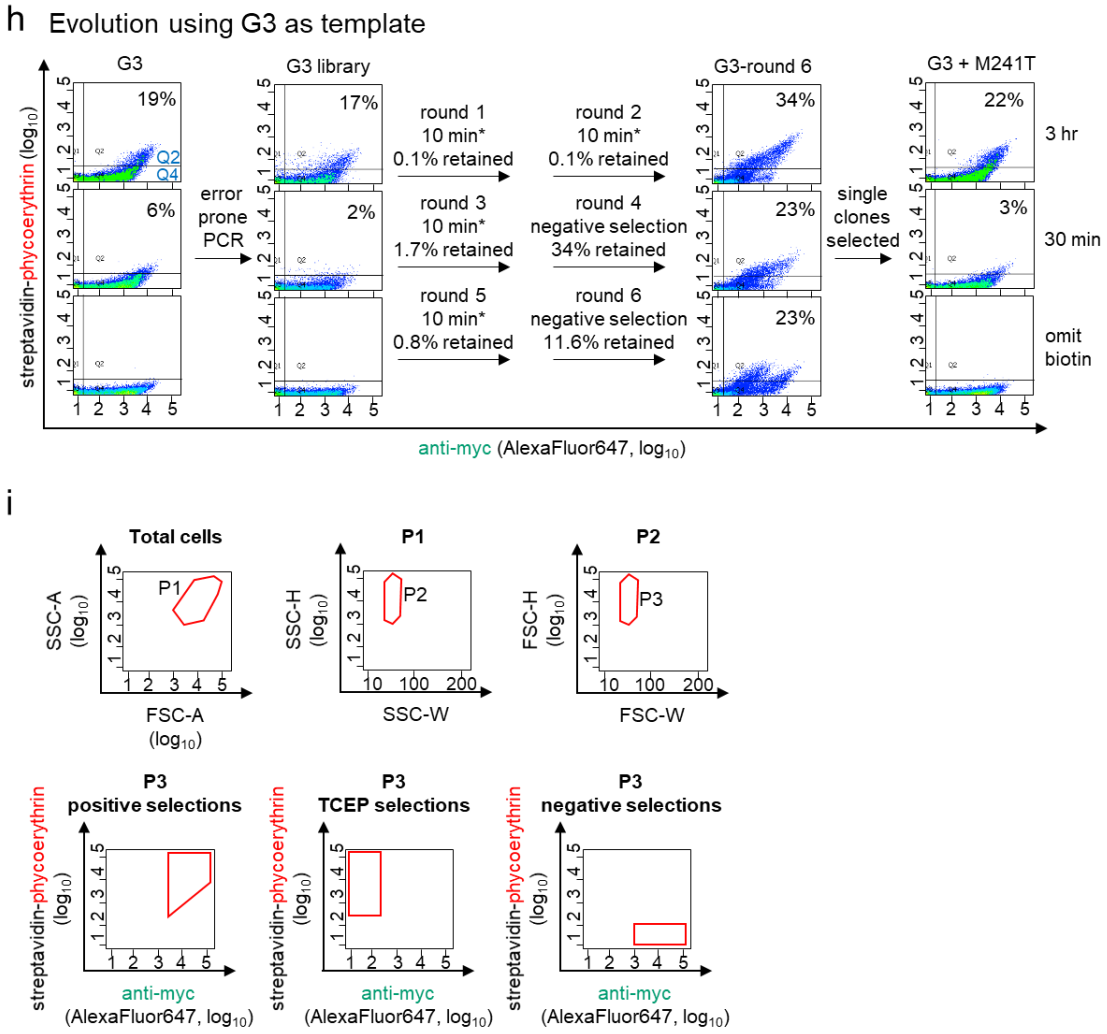

Supplementary Figure 3 (continued). Evolution of TurboID and miniTurbo via yeast display. For FACS plots, percentage of cells in upper right quadrant (Q2/(Q2+Q4)) shown in top right of each graph; where no percentage shown, <1%. (**h**) Evolution using full-length G3 as starting template. Six rounds of selection were performed, with rounds 4 and 6 being negative selections as in (f) to remove mutants with high biotin affinity. Asterisks denote selections performed in biotin-depleted media. Three analysis conditions (rows 1-3) also in biotin-depleted media. This experiment was performed once. Two additional mutations discovered during the evolution of miniTurbo in (g), K194I and S263P, were introduced into G3 + M241T to generate TurboID. (**i**) Examples of various gates used for FACS sorting. Top 3 plots show gates (in red) used to analyze single-cell yeast populations; bottom 3 plots show gates used to enrich yeast for positive selections (left), following TCEP treatment (middle), and for negative selections (right). SSC-A is side-scatter area, FSC-A is forward-scatter area, SSC-H is side-scatter height, SSC-W is side-scatter width, FSC-H is forward-scatter height, FSC-W is forward-scatter width.

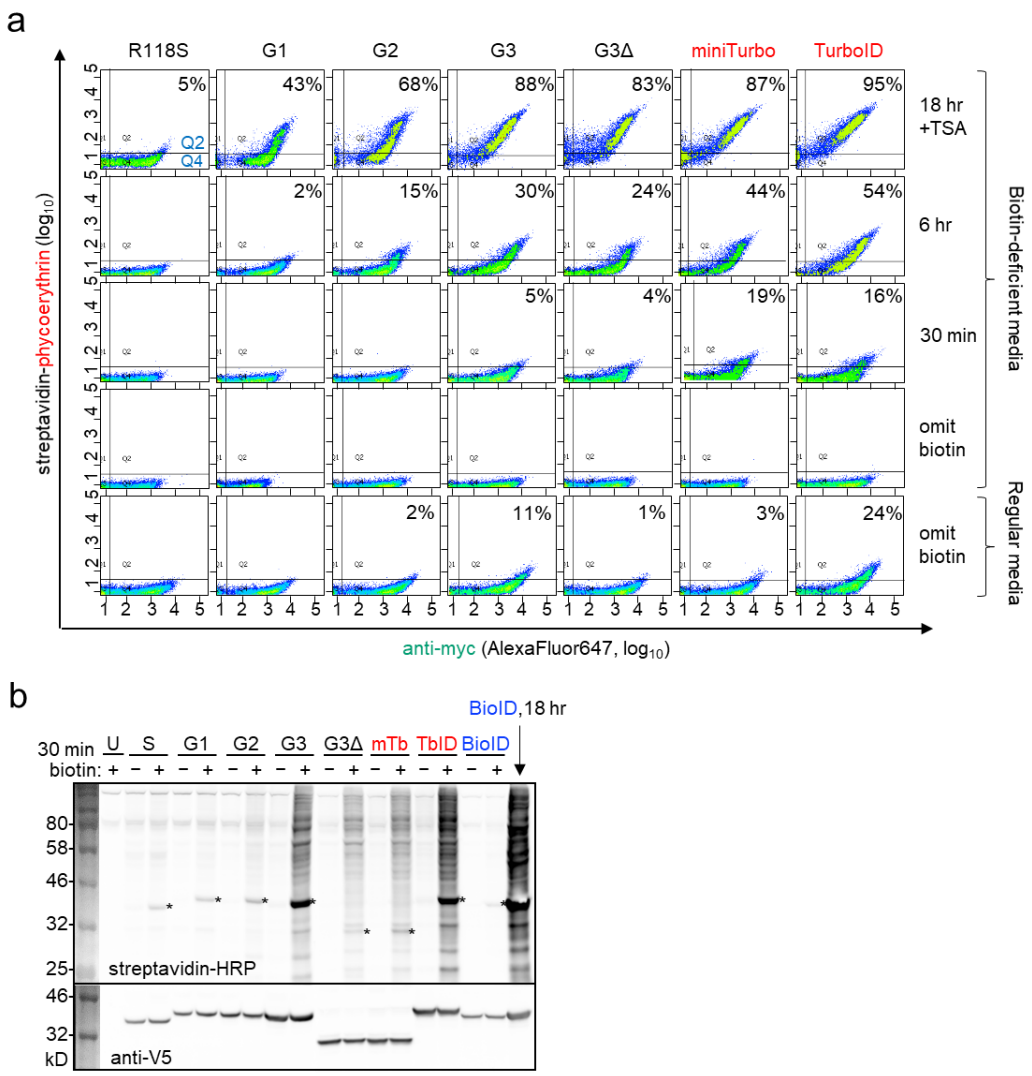

Supplementary Figure 4. **Progress of evolution.** (**a**) Yeast FACS plots summarizing the progress of evolution. Same as **Figure 1e**, but with more time points. In addition to 6 hours of labeling with 50 μM biotin, the results of 18 hr and 30 min labeling are also shown. The first four rows were carried out in biotin-depleted media, while the last row was in regular yeast media. This experiment was performed twice with similar results, except for the G3Δ samples and the omit biotin/biotin-deficient media condition samples, which were performed only once. (**b**) Comparison of different generation ligase activities in HEK cytosol. The indicated ligases were transiently expressed in the cytosol of HEK 239T cells. 50 μM exogenous biotin was added for 30 minutes, then whole cell lysates were analyzed by streptavidin blotting. Ligase expression detected by anti-V5 blotting. U, untransfected. S, BirA-R118S. Asterisks indicate ligase self-biotinylation. BioID labeling for 18 hours shown in the last lane for comparison. This experiment was performed twice with similar results. Quantitation for this experiment and its replicate shown in **Figure 1g**.

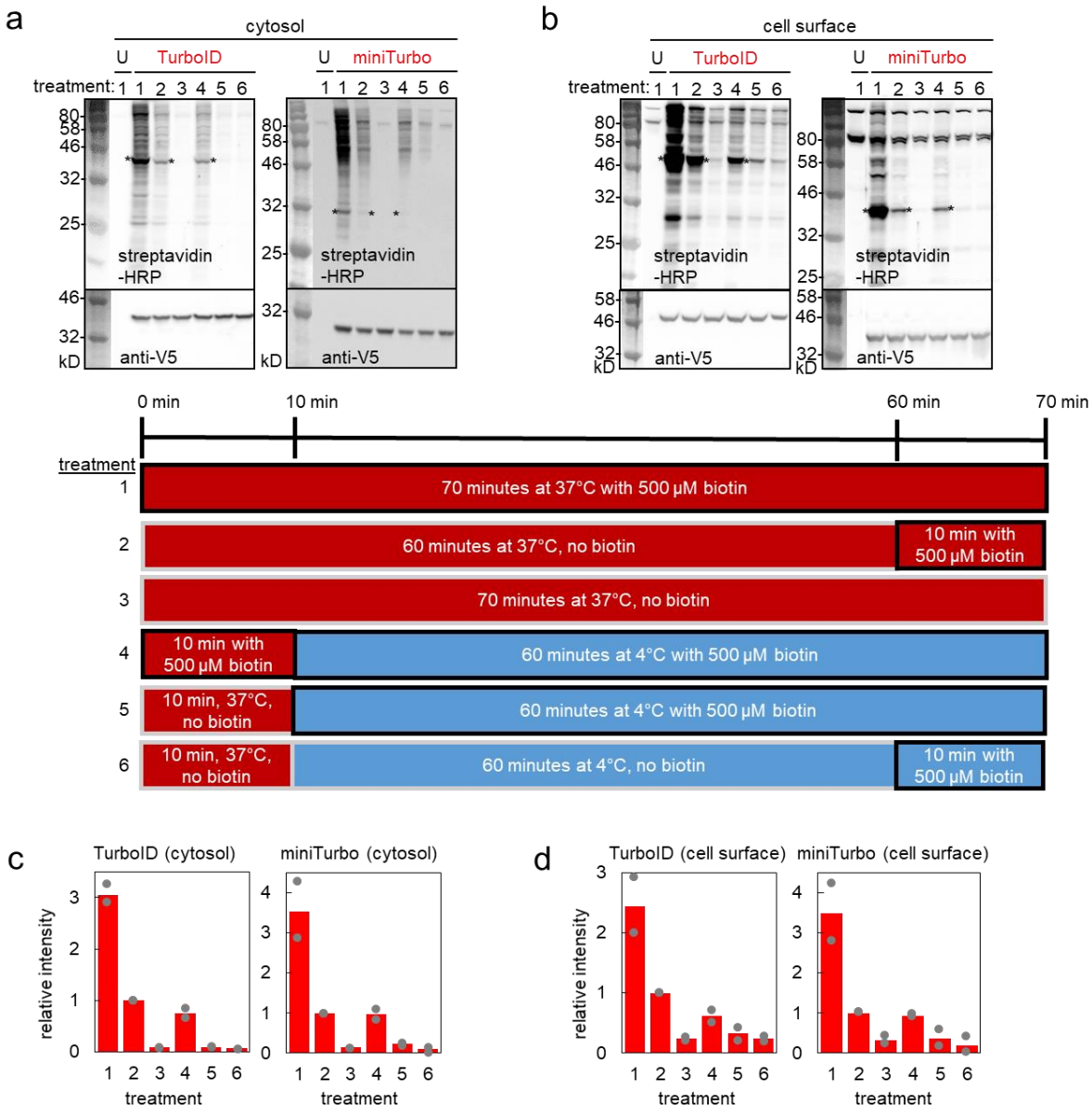

Supplementary Figure 5. **Cooling samples to 4°C terminates ligase-catalyzed biotinylation.** The indicated ligases were transiently expressed in HEK 293T cytosol (**a**) or on the cell surface (**b**). Labeling conditions (1)-(6) shown below. For (b), 0.5 mM ATP and 1.25 mM magnesium acetate were also added to cells during labeling. After labeling, whole cell lysates were analyzed by streptavidin blotting. Ligase expression detected by anti-V5 blotting. U, untransfected. Asterisks indicate ligase self-biotinylation. This experiment was performed twice with similar results. (**c, d**) Quantitation of streptavidin blot data in (a) and (b), respectively. Quantitation excludes ligase self-biotinylation band. Sum intensity of each lane is divided by the sum intensity of the ligase expression band, and the results are normalized to that of condition 2 for each ligase, which is set to 1.0. Grey dots indicate quantitation of signal intensity from each replicate, red bars indicate mean signal intensity calculated from the two replicates.

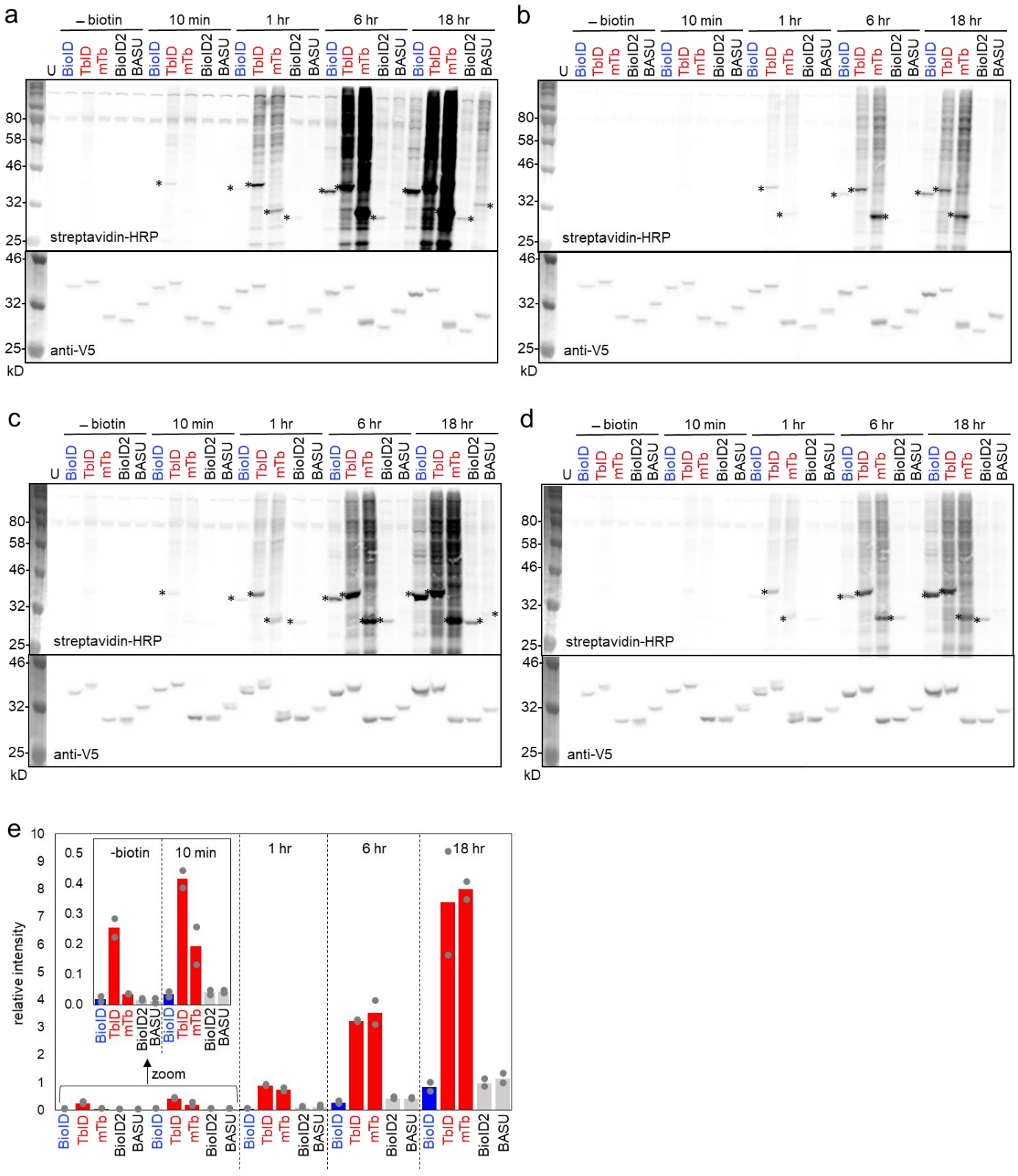

Supplementary Figure 6. **Further comparison of ligase activities in HEK cytosol.** Same as **Figure 2a**, but (a) shows the same blot with longer exposure, and (b) shows the same blot with shorter exposure. This experiment was performed twice with similar results, as indicated in **Figure 2a**. (**c, d**) Same as Figure 2a and (a, b), but labeling was with 50 μM biotin instead of 500 μM. (d) is the same as (c), but with shorter exposure time. This experiment was performed twice with similar results. (**e**) Quantitation of streptavidin blot data presented in (c, d). Longer exposure shown in (c) used to quantify '–biotin' and '10 minute' samples; shorter exposure shown in (d) used to quantify '1 hr', '6 hr', and '18 hr' samples. Intensity:expression ratios are normalized to that of BioID, 18 hours, as in **Figure 1g**.

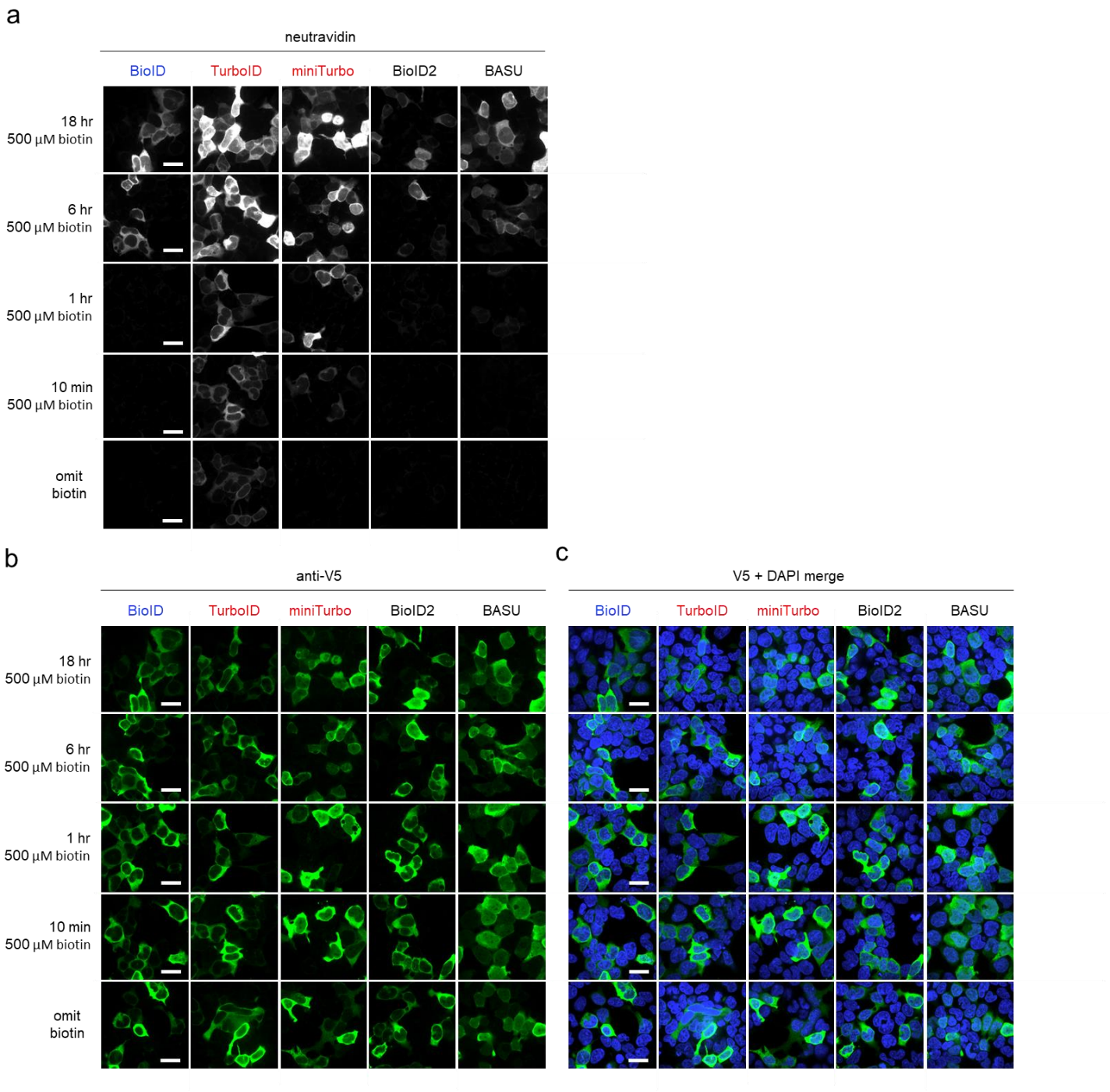

Supplementary Figure 7. Comparison of ligase activities in HEK cytosol by fluorescence microscopy. The indicated ligases were transiently expressed in the cytosol of HEK 293T cells. 500 µM exogenous biotin was added for 18 hr, 6 hr, 1 hr, or 10 minutes, then cells were fixed and stained with (**a**) neutravidin-AlexFluor647 to visualize biotinylated proteins, (**b**) anti-V5 (green) to visualize ligase expression, and (**c**) DAPI (blue) to visualize nuclei. Scale bars, 10 µm. This experiment was performed twice with similar results.

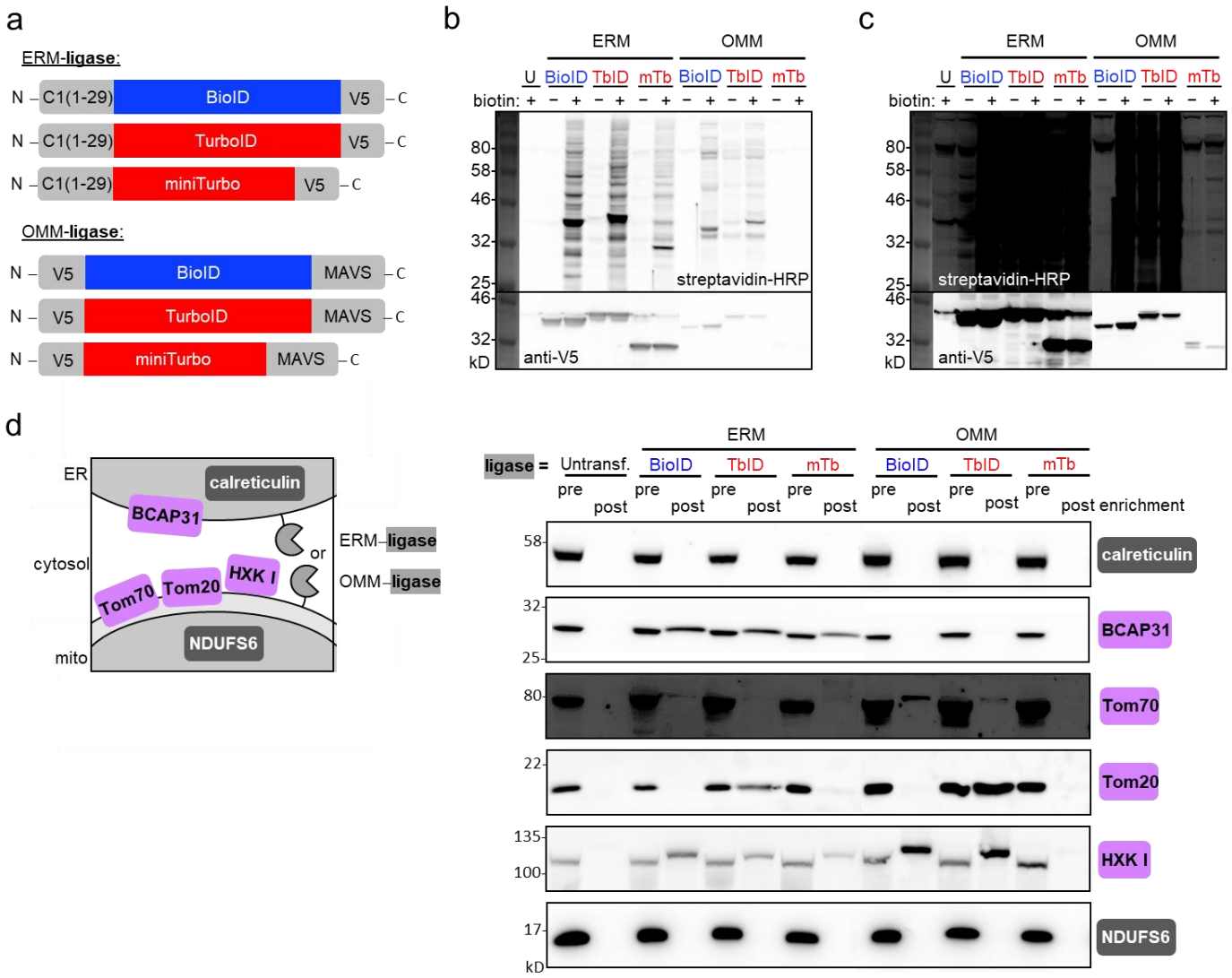

Supplementary Figure 8. Proximity labeling with BioID, TurboID, and miniTurbo at the ER and mitochondrial membranes. (**a**) Constructs targeting the ligases to the ER membrane (ERM), facing cytosol, and to the outer mitochondrial membrane (OMM), facing cytosol. ERM targeting sequence is derived from cytochrome P450 (C1(1-29)); OMM targeting sequence is from the C-terminal 31 amino acids of MAVS (mitochondrial antiviral signaling protein). See **Supplementary Table 8** for more details. (**b**) Streptavidin blots showing promiscuous biotinylation by the indicated ligases, in live HEK 293T cells. BioID labeling was for 18 hours (50 μM biotin), while TurboID and miniTurbo labeling were for 10 minutes (500 μM biotin). Anti-V5 quantifies ligase expression levels. This experiment was performed twice with similar results. (**c**) Same as (b) but with longer exposure. (**d**) Blotting of streptavidin-enriched lysates from (b) with antibodies against the six endogenous marker proteins shown (calreticulin in the ER lumen, NDUFS6 in the mitochondrial matrix, BCAP31 on the ERM facing cytosol, and Tom70, Tom20, and hexokinase I (HXK I) on the OMM facing cytosol). “Pre” indicates whole cell lysate, pre-streptavidin enrichment. “Post” indicates lysate after streptavidin bead enrichment and elution. This experiment was performed twice with similar results.

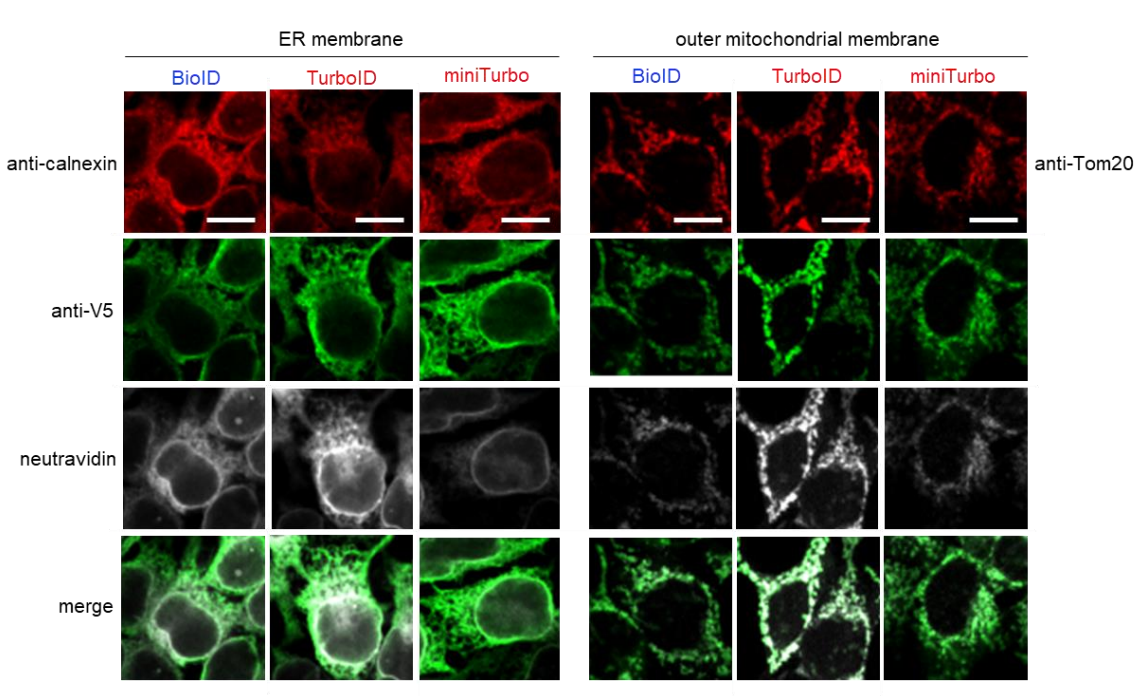

Supplementary Figure 8 (continued). Proximity labeling with BioID, TurboID, and miniTurbo at the ER and mitochondrial membranes. (**e**) Characterization of biotin-labeled cells by fluorescence microscopy. HEK cells were transduced with the constructs in (a), via lentivirus, and labeled as in (b). After fixation, cells were stained with neutravidin-AlexFluor647 to visualize biotinylated proteins, anti-V5 to visualize ligase expression, anti-calnexin to stain ER, and anti-Tom20 antibody to stain mitochondria. Scale bars, 10 μm. This experiment was performed twice with similar results.

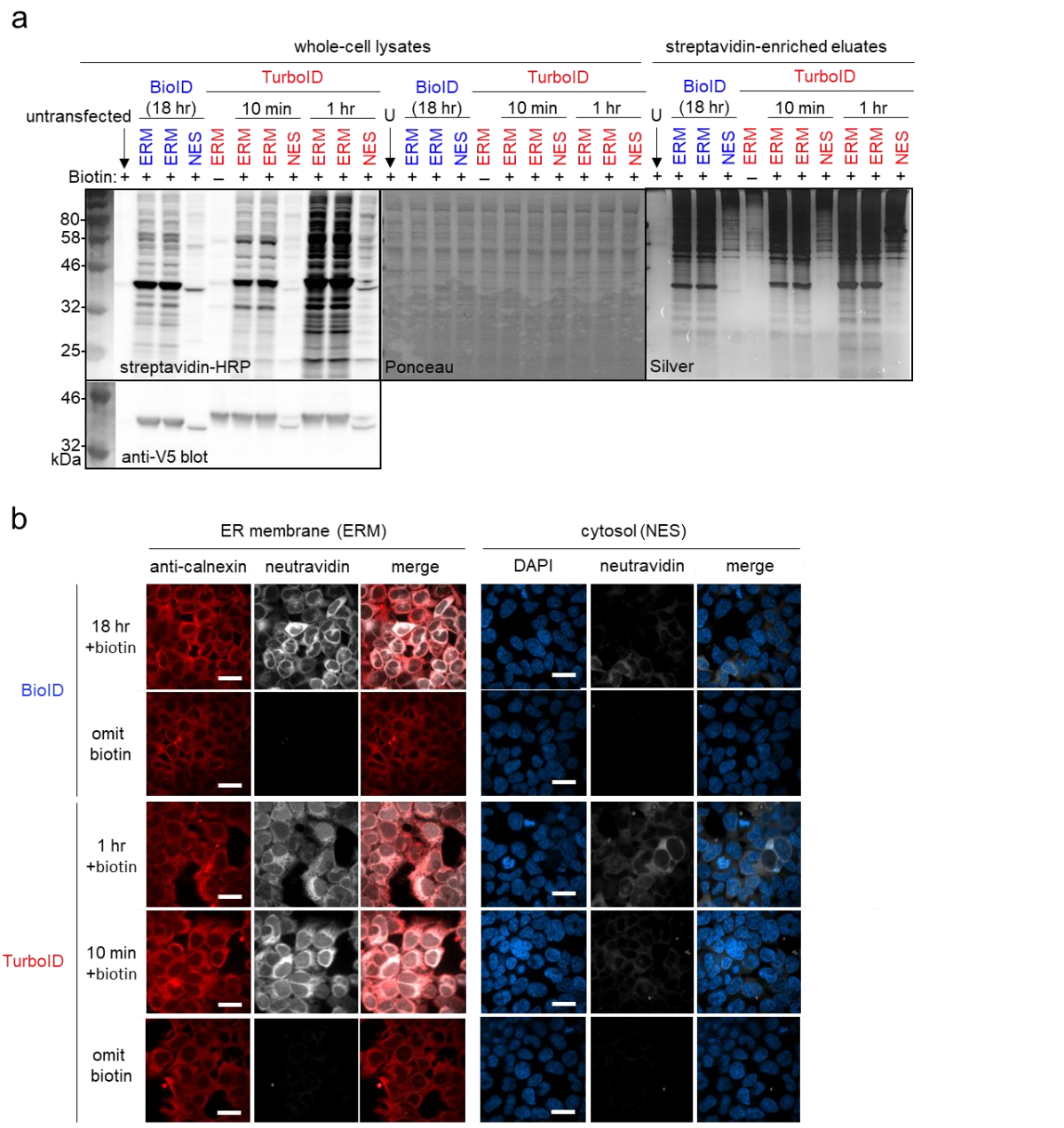

Supplementary Figure 9. Additional data for the ER membrane proteomic experiment. Related to **Figure 2d-g**. (**a**) Western blot and gel characterization of proteomic samples from **Figure 2d**. 2.5% of each whole cell lysate was used for streptavidin blotting and anti-V5 blotting at left. Ponceau staining (middle) shows equal loading of samples. U, untransfected. Right: 5% of streptavidin beads were boiled in SDS buffer to elute biotinylated proteins. Eluted proteins were separated on SDS-PAGE and detected by silver stain. This experiment was performed once alongside the proteomic experiment, and also performed once separately on a smaller scale with similar results. (**b**) Characterization of proteomic samples by fluorescence microscopy. HEK prepared and labeled as in **Figure 2d** were fixed and stained with neutravidin-AlexFluor647 to visualize biotinylated proteins, anti-calnexin to stain ER, and DAPI to stain nuclei. Scale bars, 20 μm. This experiment was performed twice with similar results.

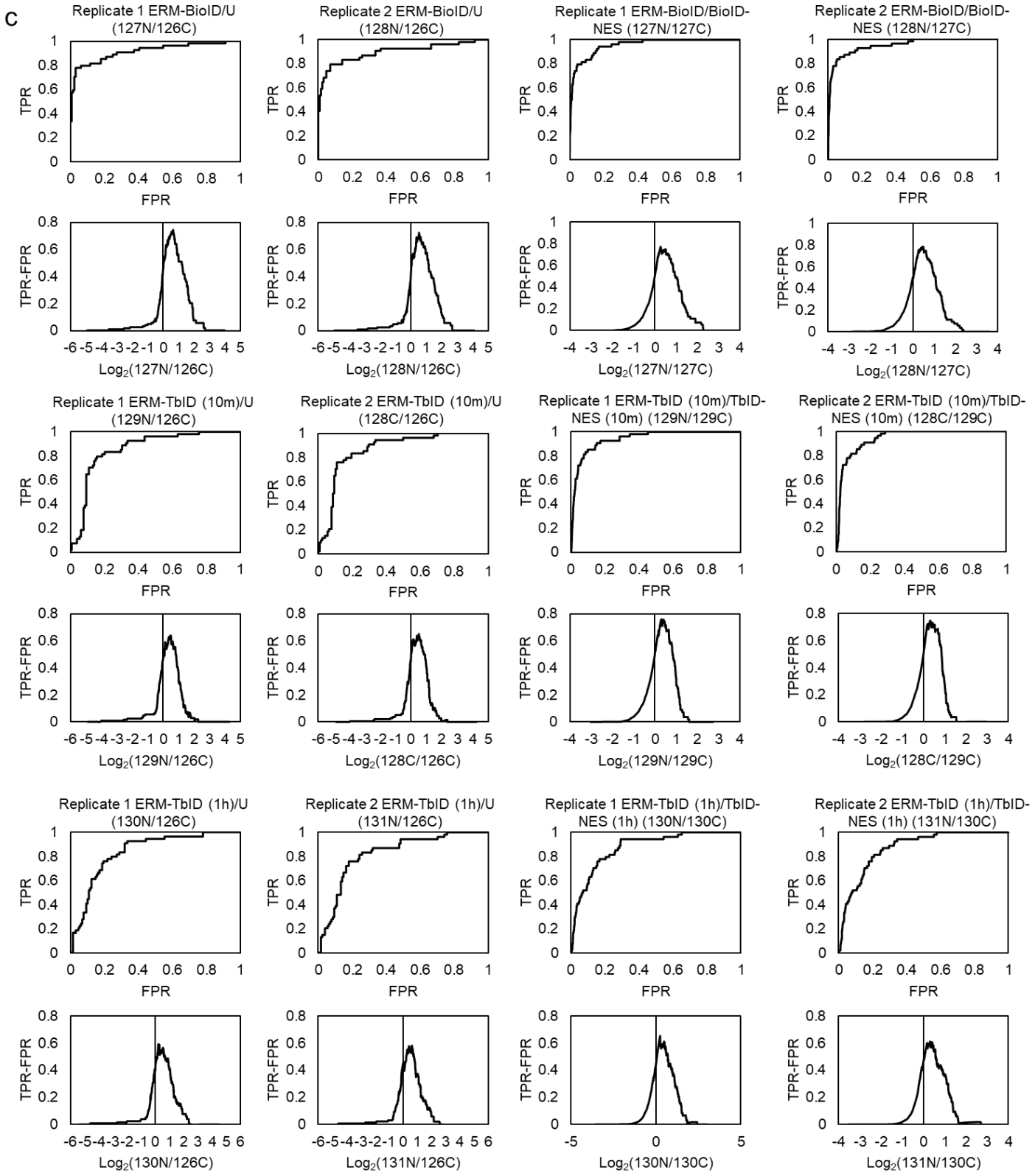

Supplementary Figure 9 (continued). Additional data for the ER membrane proteomic experiment. Related to **Figure 2d-g**. (**c**) ROC (receiver operating characteristic) analysis to determine TMT ratio cut-offs to generate final proteomic datasets. For every possible TMT ratio cutoff, the true positive rate (TPR) was plotted against the false positive rate (FPR) in a (ROC) curve. TPR is defined as the fraction of detected true positive proteins above the cutoff. FPR is defined as the fraction of detected false positive proteins above the cutoff. The bottom graph plots the difference between the TPR and FPR at every TMT ratio cutoff. Cutoff is made at the TMT ratio at which TPR-FPR is maximal, and it is depicted in the histograms in (d) and scatter plots in (e) as a dashed line. This analysis was performed using the entire dataset.

d

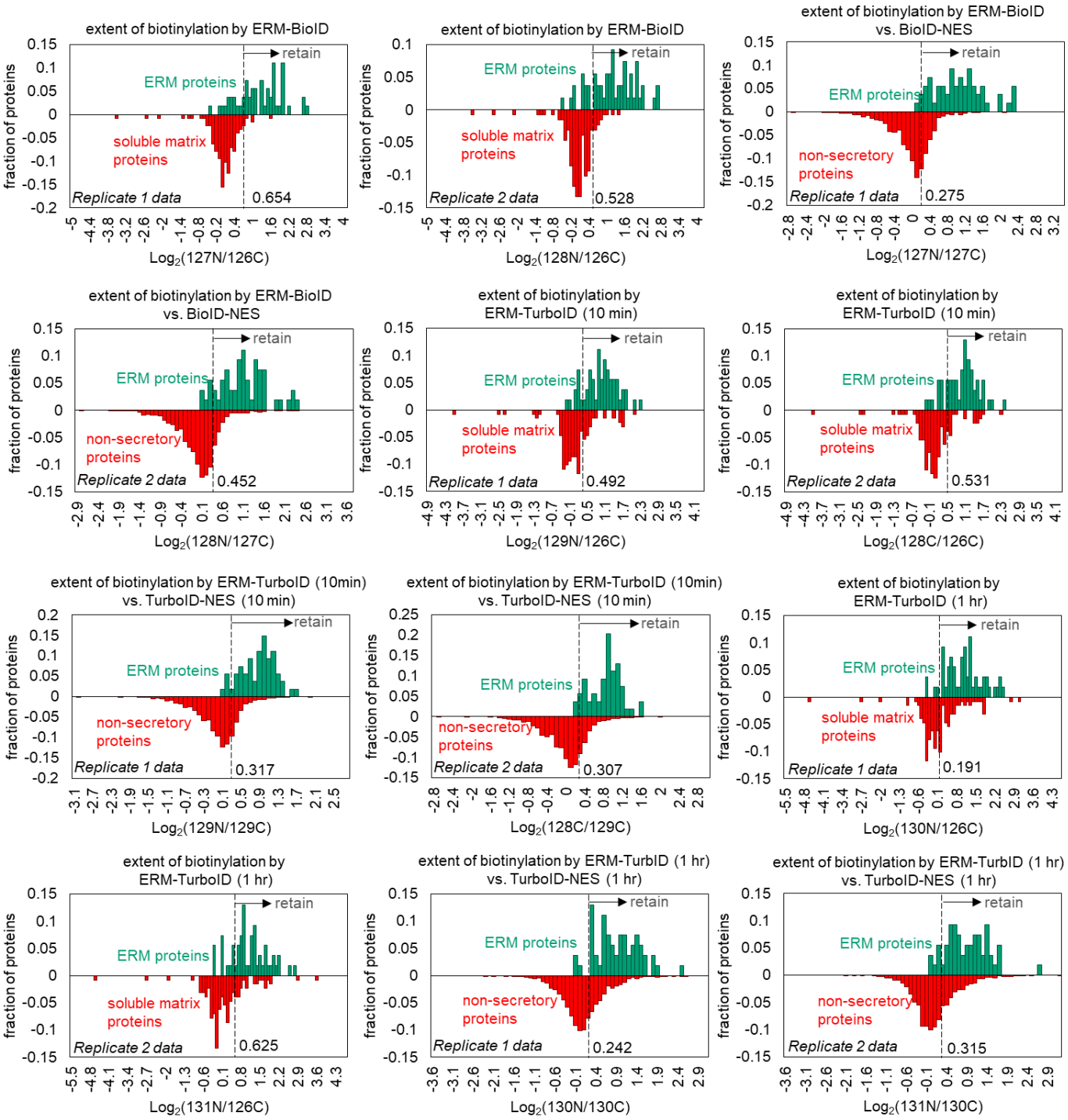

Supplementary Figure 9 (continued). Additional data for the ER membrane proteomic experiment. Related to **Figure 2d-g**. (**d**) Histograms showing the distribution of true positives (green; e.g., proteins with prior ER membrane annotation, **Supplementary Table 2 Tab 1**) and false positives (red; e.g., soluble mitochondrial matrix proteins that should not be labeled by ERM-ligase fusions, **Supplementary Table 2 Tabs 2, 3**) by TMT ratio. Dashed vertical lines show TMT ratio cut-offs determined by ROC analysis in (c) and applied to the entire dataset to generate final proteomes.

e

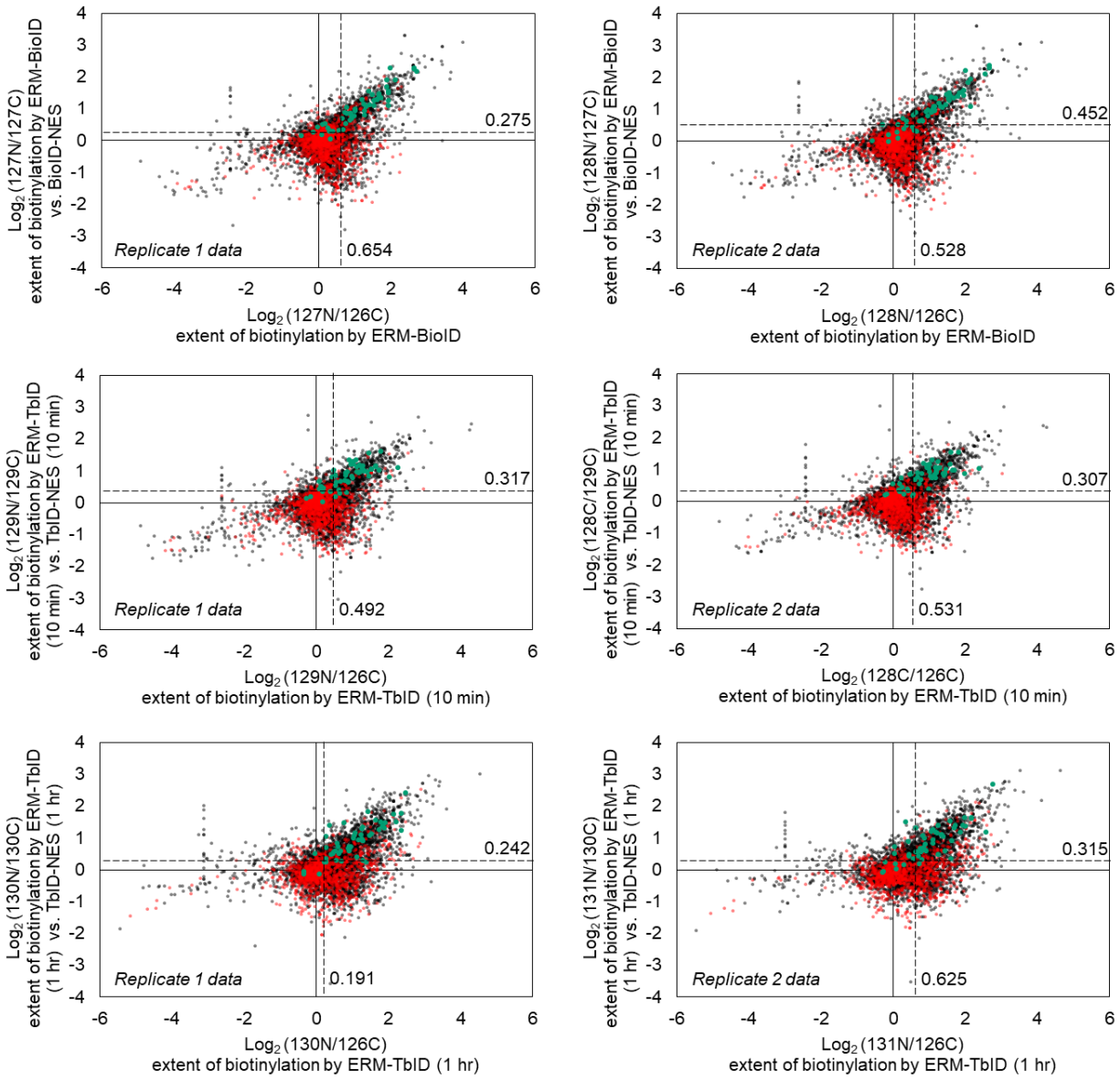

Supplementary Figure 9 (continued). Additional data for the ER membrane proteomic experiment. Related to **Figure 2d-g**. (**e**) Scatter plots showing $\log_2$(ERM/NES) versus $\log_2$(ERM/untransfected) for each proteomic experiment. Known ERM proteins (from our ERM true positive list, **Supplementary Table 2 Tab 1**) are shown in green; proteins with cytosolic annotation are shown in red (i.e., potential false positives, **Supplementary Table 2 Tab 7**); all other proteins are shown in black. Dashed lines show TMT ratio cut-offs.

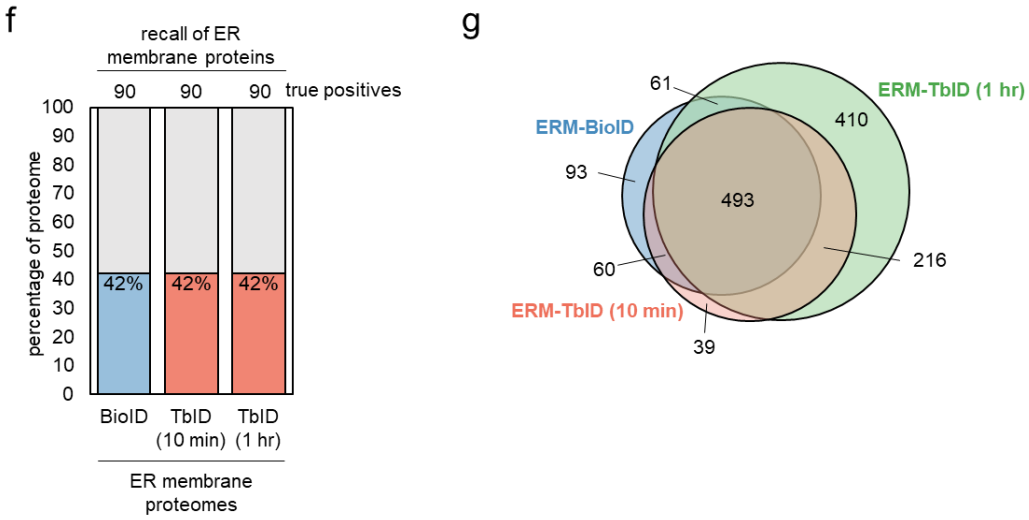

Supplementary Figure 9 (continued). Additional data for the ER membrane proteomic experiment. Related to **Figure 2d-g**. (**f**) Coverage analysis for each proteomic dataset. Graph indicates the fraction of true positive proteins found in each proteome. True positive proteins used for this analysis were curated from literature and listed in **Supplementary Table 2 Tab 1** (size of this list is shown across top). (**g**) Overlap of BioID (blue), TurboID 10 minute (orange) and TurboID 1 hour (green)-derived ERM proteomes.

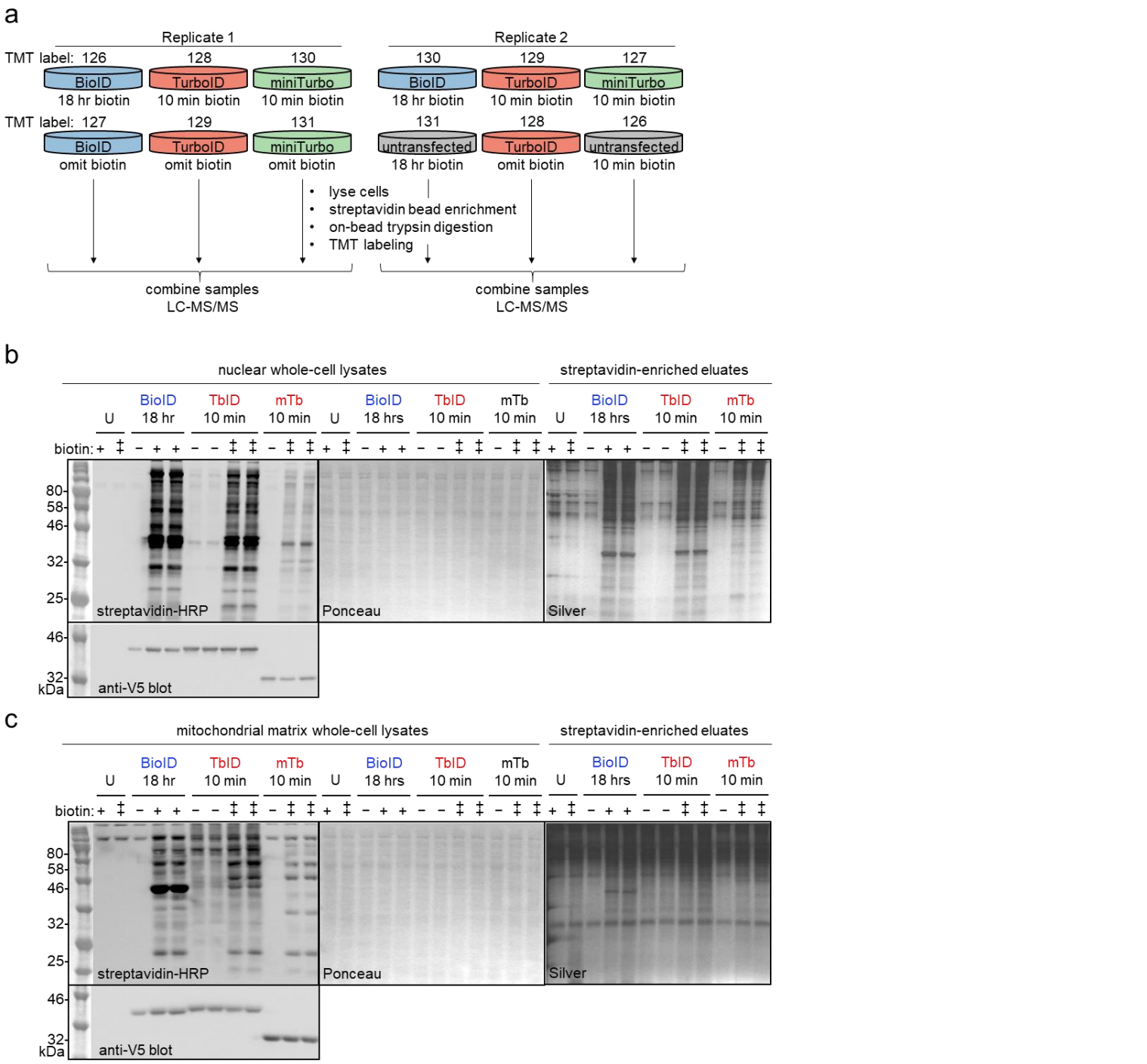

Supplementary Figure 10. Nuclear and mitochondrial matrix proteomes obtained via BioID, TurboID, and miniTurbo-catalyzed labeling. Related to **Figure 2h.** (**a**) Mass spectrometry-based proteomic experiment comparing BioID, TurboID, and miniTurbo in the nucleus or mitochondrial matrix. Experimental design and labeling conditions. Ligase fusion constructs were transiently expressed for the nuclear samples and stably expressed for the mitochondrial matrix samples in HEK 239T. BioID samples were treated with 50 μM biotin for 18 hours, while TurboID and miniTurbo samples were treated with 500 μM biotin for 10 minutes. After labeling, cells were lysed and biotinylated proteins were enriched with streptavidin beads, digested to peptides, and conjugated to TMT (tandem mass tag) labels. All 6 samples in each replicate were then combined and analyzed by LC-MS/MS. This experiment was performed once with two replicates per condition. **(b, c)** Western blot and gel characterization of proteomic samples from (a) for (b) nucleus and (c) mitochondrial matrix proteomic experiments. 2.5% of each whole cell lysate was used for streptavidin blotting and anti-V5 blotting at left. Ponceau staining (middle) shows equal loading of samples. U, untransfected. Right: 5% of streptavidin beads were boiled in SDS buffer to elute biotinylated proteins. Eluted proteins were separated on SDS-PAGE and detected by silver stain. These experiments were each performed once alongside the proteomic experiment, and also each performed once separately on a smaller scale with similar results.

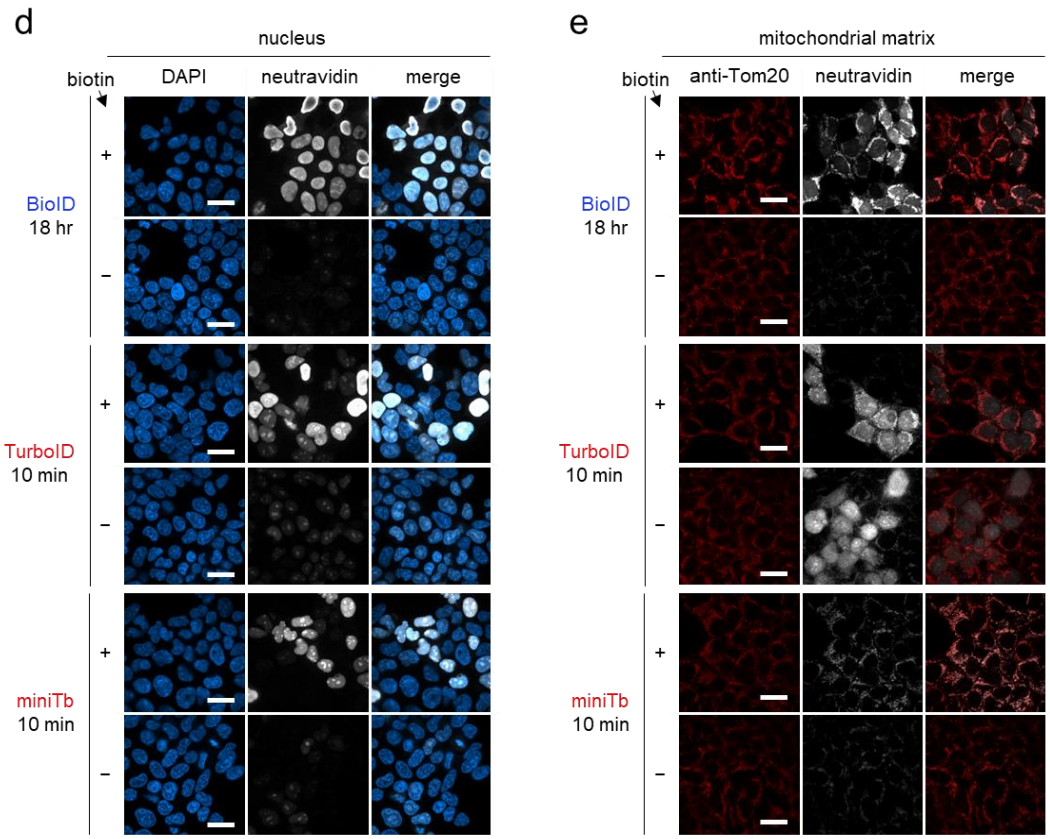

Supplementary Figure 10 (continued). Nuclear and mitochondrial matrix proteomes obtained via BioID, TurboID, and miniTurbo-catalyzed labeling. Related to **Figure 2h.** (**d, e**) Characterization of (d) nuclear and (e) mitochondrial matrix proteomic samples by fluorescence microscopy. HEK prepared and labeled as in (a) were fixed and stained with neutravidin-AlexFluor647 to visualize biotinylated proteins, DAPI to stain nuclei in (d), and anti-Tom20 antibody to stain mitochondria in (e). Scale bars, 20 μm. These experiments were each performed twice with similar results.

f

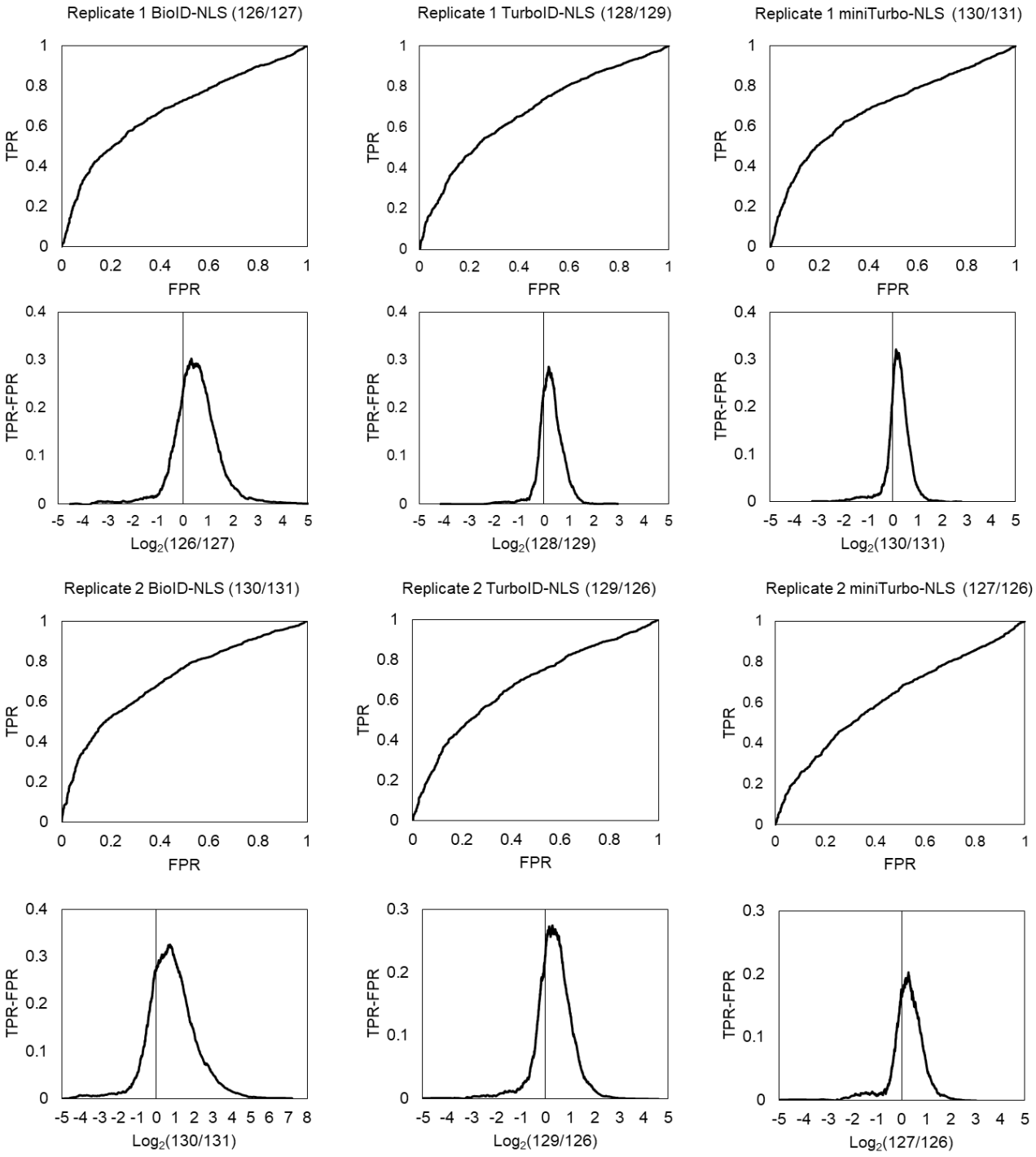

Supplementary Figure 10 (continued). Nuclear and mitochondrial matrix proteomes obtained via BioID, TurboID, and miniTurbo-catalyzed labeling. Related to **Figure 2h.** (**f**) ROC analysis as in **Supplementary Figure 9c** for nuclear samples. This analysis was performed using the entire datasets.

g

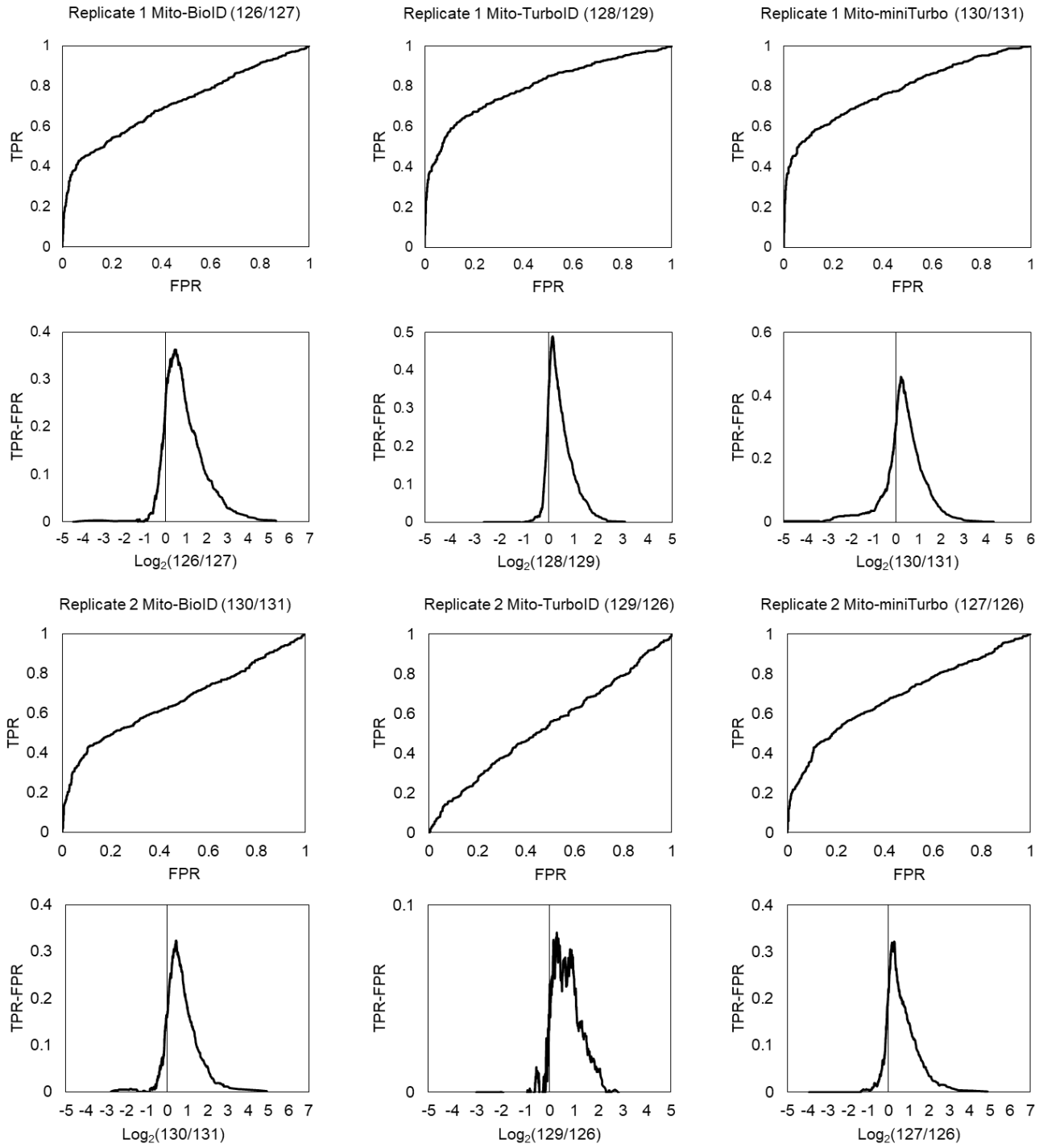

Supplementary Figure 10 (continued). Nuclear and mitochondrial matrix proteomes obtained via BioID, TurboID, and miniTurbo-catalyzed labeling. Related to **Figure 2h.** (**g**) ROC analysis as in **Supplementary Figure 9c** for mitochondrial matrix samples. This analysis was performed using the entire datasets.

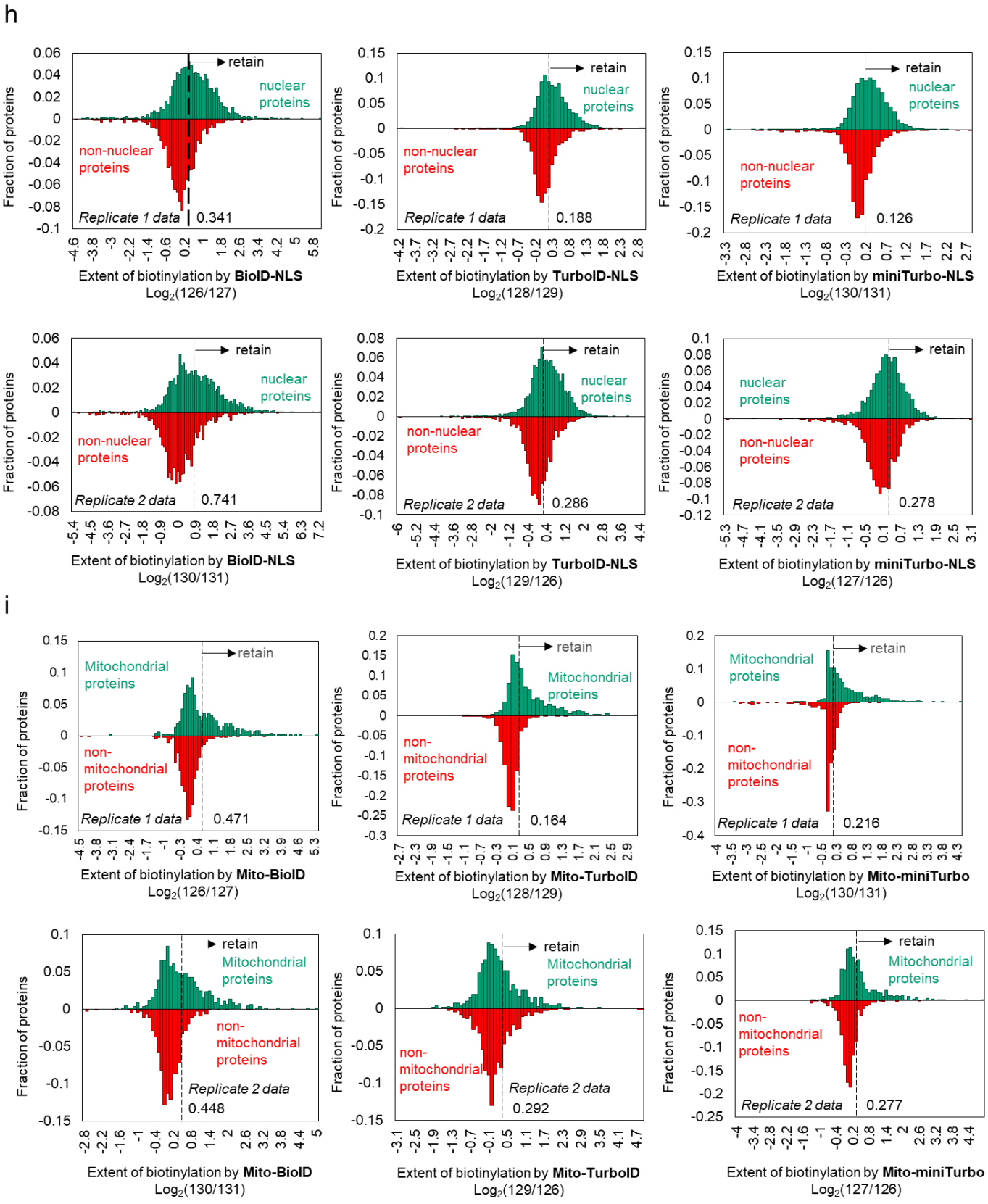

Supplementary Figure 10 (continued). Nuclear and mitochondrial matrix proteomes obtained via BioID, TurboID, and miniTurbo-catalyzed labeling. Related to **Figure 2h.** (**h, i**) Histograms as in **Supplementary Figure 9d** for (h) nuclear samples and (i) mitochondrial matrix samples.

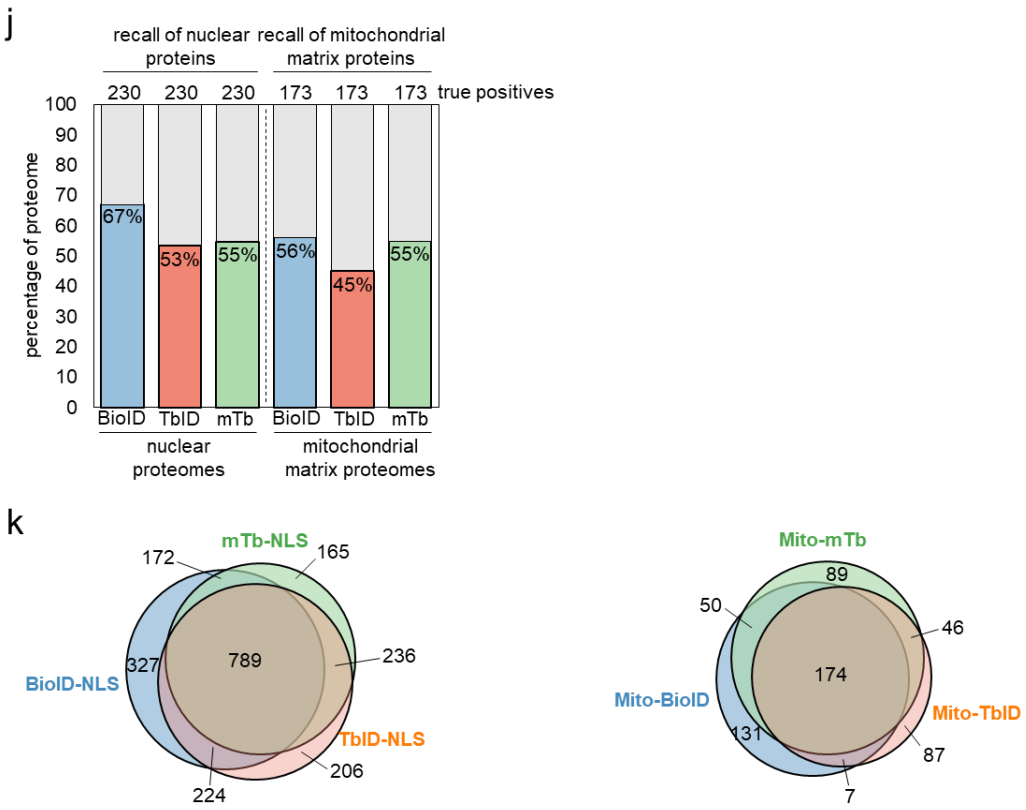

Supplementary Figure 10 (continued). Nuclear and mitochondrial matrix proteomes obtained via BioID, TurboID, and miniTurbo-catalyzed labeling. Related to **Figure 2h.** (**j**) Coverage analysis as in **Supplementary Figure 9f**. True positive proteins used for this analysis were curated from literature and listed in **Supplementary Table 3 Tab 3** for nuclear experiment and **Supplementary Table 4 Tab 3** for mitochondrial matrix experiment (sizes of each list shown across top). (**k**) Overlap of BioID (blue), TurboID (orange) and miniTurbo (green)-derived proteomes for the nucleus (left) and mitochondrial matrix (right).

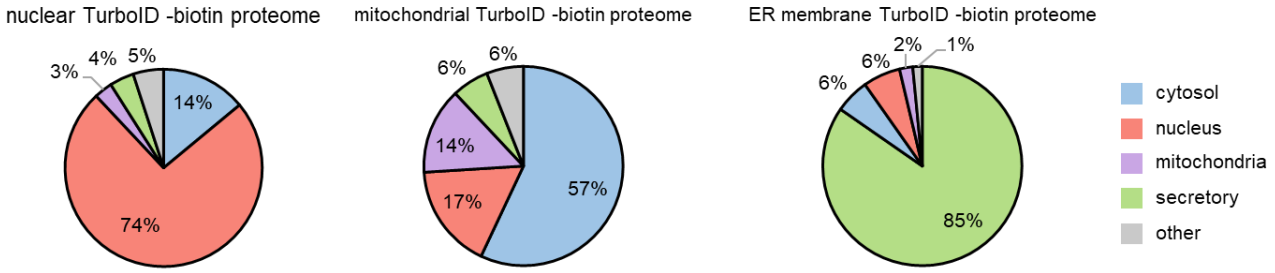

Supplementary Figure 11. Proteins biotinylated by TurboID prior to addition of exogenous biotin. We generated proteomic datasets from the control samples in which TurboID fusion constructs were expressed but biotin was withheld ("omit biotin" samples). We used the same ROC-based filtering as described in **Supplementary Figure 9** and **Supplementary Figure 10** to produce proteomes of 840 proteins for the ERM (**Supplementary Table 5 Tab 5**), 1540 proteins for the mitochondrial matrix (**Supplementary Table 7 Tab 5**), and 993 proteins for the nucleus (**Supplementary Table 6 Tab 5**). The pie charts show the GOCC[3,4] subcellular classifications for each "-biotin" proteome.

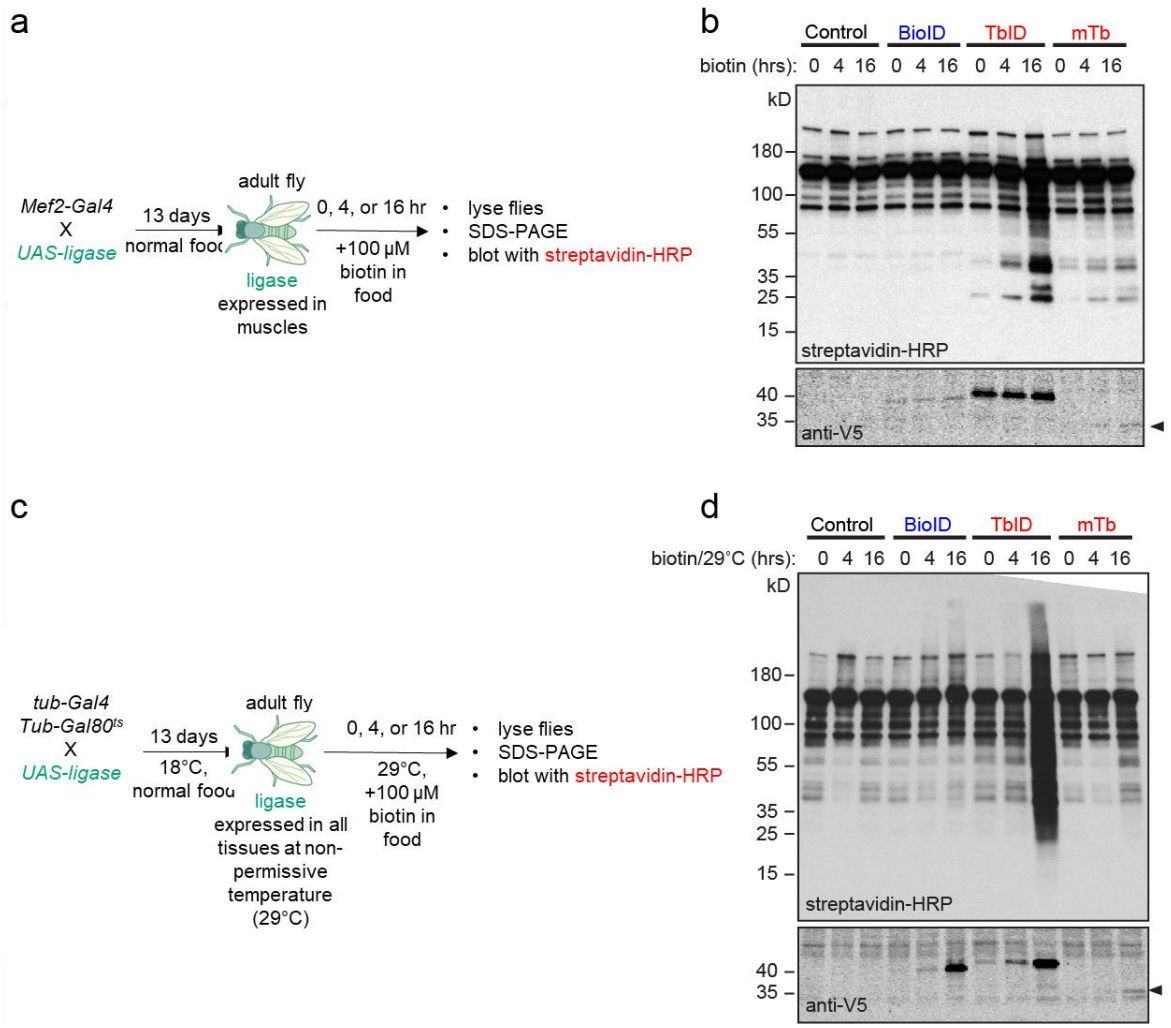

Supplementary Figure 12. Further comparison of ligase activities in *D. melanogaster*. (**a**) *Mef2-Gal4* drives expression of UAS-ligase in muscles at all developmental time points. Flies were raised on normal food for 13 days after egg deposition, then adults were transferred to food supplemented with 100 µM biotin for the time indicated, and whole adult flies were lysed. (**b**) Western blotting of adult fly lysates described in (a). Biotinylated proteins detected by blotting with streptavidin-HRP, and ligase expression detected by anti-V5 blotting. This experiment was performed twice with similar results. (**c**) *Tub-Gal4* drives ubiquitous expression of UAS-ligases in all cells at all developmental time points, but is silenced by *tub-Gal80ts* at the permissive temperature (18˚C). Incubating flies at non-permissive temperature (29˚C) inhibits Gal80, and induces expression of indicated *UAS-ligase* enzyme. Flies were raised on normal food for 13 days after egg deposition, then adults were transferred to food supplemented with 100 µM biotin for the time indicated. (**d**) Western blotting of adult fly lysates described in (c). Biotinylated proteins detected by blotting with streptavidin-HRP, and ligase expression detected by anti-V5 blotting. This experiment was performed twice with similar results. For (b) and (d), control sample is *UAS-Luciferase*, and arrowheads indicate V5-miniTurbo band.

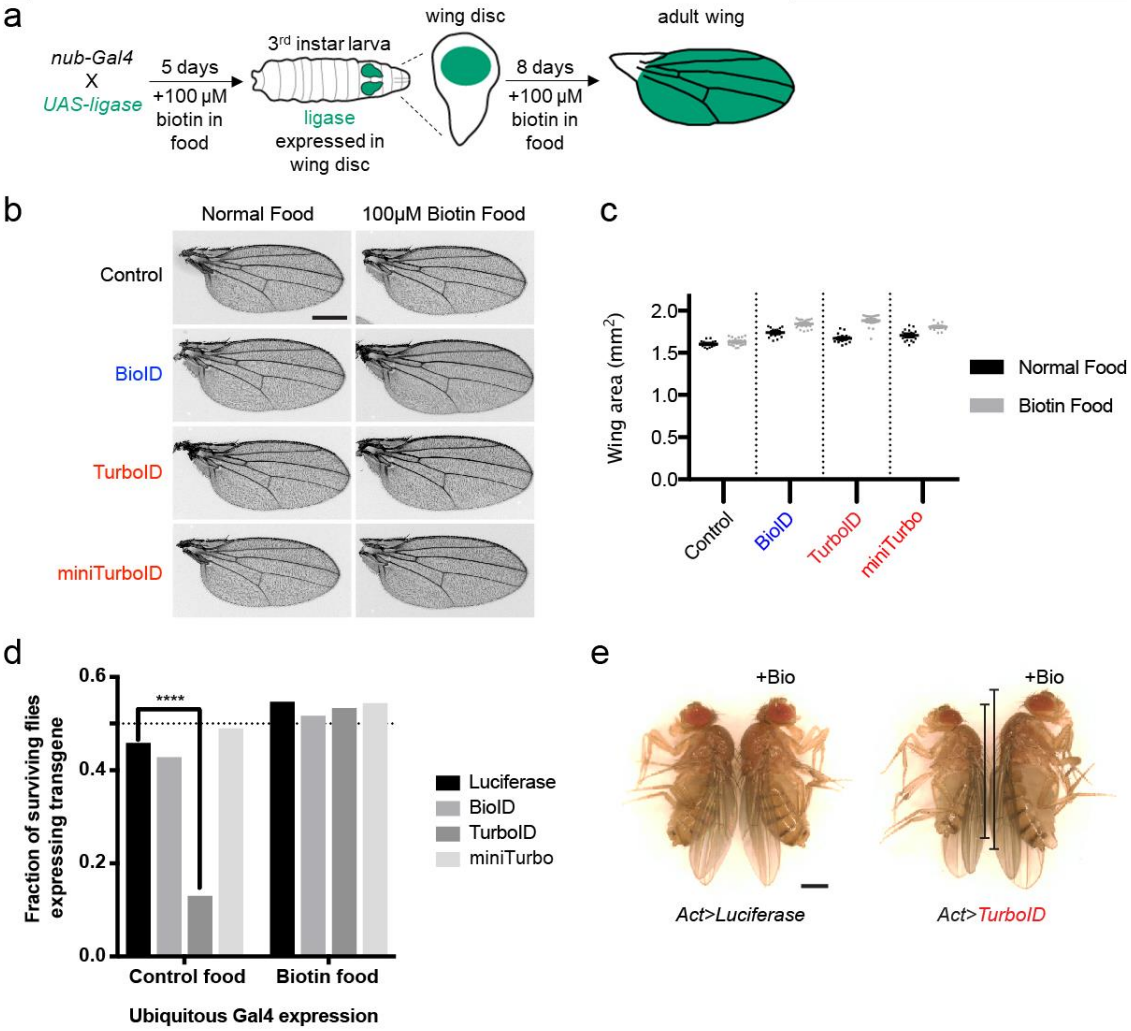

Supplementary Figure 13. Morphology and viability assays in *D. melanogaster* expressing promiscuous biotin ligases. (**a**) *nub-Gal4* drives expression of the indicated *UAS-ligase* in the wing disc pouch, which gives rise to the adult wing blade. Flies were provided food supplemented with 100 µM biotin for 13 days after egg deposition, then the wings were dissected from adult flies. (**b**) Images of adult female wings as prepared in (a). Control flies are *nub-Gal4* crossed with a wild-type strain (*w1118*). Flies were raised on control food, or on food supplemented with 100 µM biotin. Scale bar is 0.5 mm. This experiment was repeated twice with similar results. (**c**) Quantitation of wing area of specimens prepared as described in (a) and (b). Sample size values (n) from left column to right: 17, 14, 17, 15, 19, 18, 19, 18. The indicted measure of center shows the mean. Error bars in s.e.m. This experiment was performed three times with similar results. (**d**) Viability assay by quantification of flies surviving to adulthood. *UAS-Luciferase* (control) or *UAS-ligase* transgenes (experimental) were expressed ubiquitously during development using *Actin-Gal4*. Throughout development, flies were raised on normal fly food or food supplemented with 100 µM biotin. Graph shows the fraction of adult flies expressing UAS-transgenes (# flies expressing UAS-transgene/(# flies expressing UAS-transgene + # sibling control flies)). Dashed line indicates the expected Mendelian segregation frequency (0.5) if *UAS-transgene* expression is non-toxic. For each food type, a two-sided Chi-square test was used to determine if the difference in proportions (measure of effect) of *UAS-ligase* transgenes to *UAS-Luciferase* was statistically significant. ****, p <0.0001. All other pairwise comparisons were not statistically significant (p value >0.05). P values for all data points – Columns 1/2: 0.3113, Columns 1/3: <0.0001, Columns 1/4: 0.3027, Columns 5/6: 0.4109, Columns 5/7: 0.718, Columns 5/8: 0.9369. Sample size values (n) from left column to right: 512, 586, 466, 563, 286, 524, 513, 459. 95% confidence intervals (CI) for the difference in proportions of BioID, TurboID, and miniTurboID compared to Luciferase were -0.02945 to 0.09046, 0.2757 to 0.384, and -0.02958 to 0.09206 for normal food, and -0.04278 to 0.104, -0.05999 to 0.08728, and -0.07191 to 0.07838 for biotin food. This experiment was performed twice with similar results. (**e**) Image of adult *Act-Gal4*/*UAS-Luciferase* flies and adult *Act-Gal4*/*UAS-TurboID* flies from (d) that are grown on control food and food supplemented with 100 µM biotin (+Bio). Vertical black lines illustrate size difference between flies expressing TurboID that are raised on normal food versus biotin food. Adult flies shown are female. This experiment was repeated three times with similar results.

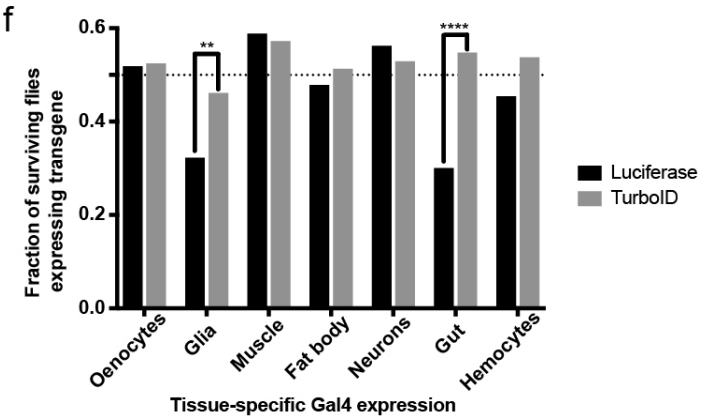

Supplementary Figure 13 (continued). Morphology and viability assays in *D. melanogaster* expressing promiscuous biotin ligases. (**f**) Survival assays with tissue-specific expression of TurboID during development. Flies were raised on normal fly food (no biotin supplement) throughout development. Graph shows the fraction of adult flies expressing either *UAS-Luciferase* or *UAS-TurboID* versus the total number of flies (see Methods). Data was analyzed as in (d). For all of the tissue specific Gal4 lines, TurboID does not significantly decrease the fraction of surviving flies relative to Luciferase. For glia and gut *Gal4* drivers, the fraction of surviving flies expressing TurboID is statistically higher relative to Luciferase. All other comparisons were not statically significant (p value >0.05). P values for all data points – Oenocytes: 0.8719, Glia: 0.0017, Muscle: 0.7295, Fat body: 0.2333, Neurons: 0.7143, Gut: <0.0001, Hemocytes: 0.8917. Sample size values (n) from left column to right: 350, 367, 196, 339, 203, 284, 194, 287, 214, 232, 215, 305, 240, 346. 95% confidence intervals (CI) for each Gal4 line from left to right were -0.06874 to 0.0807, 0.04977 to 0.2228, -0.07546 to 0.1081, -0.03849 to 0.148, -0.07737 to 0.1115, 0.1398 to 0.3063, -0.07858 to 0.08951. This experiment was performed twice with similar results.

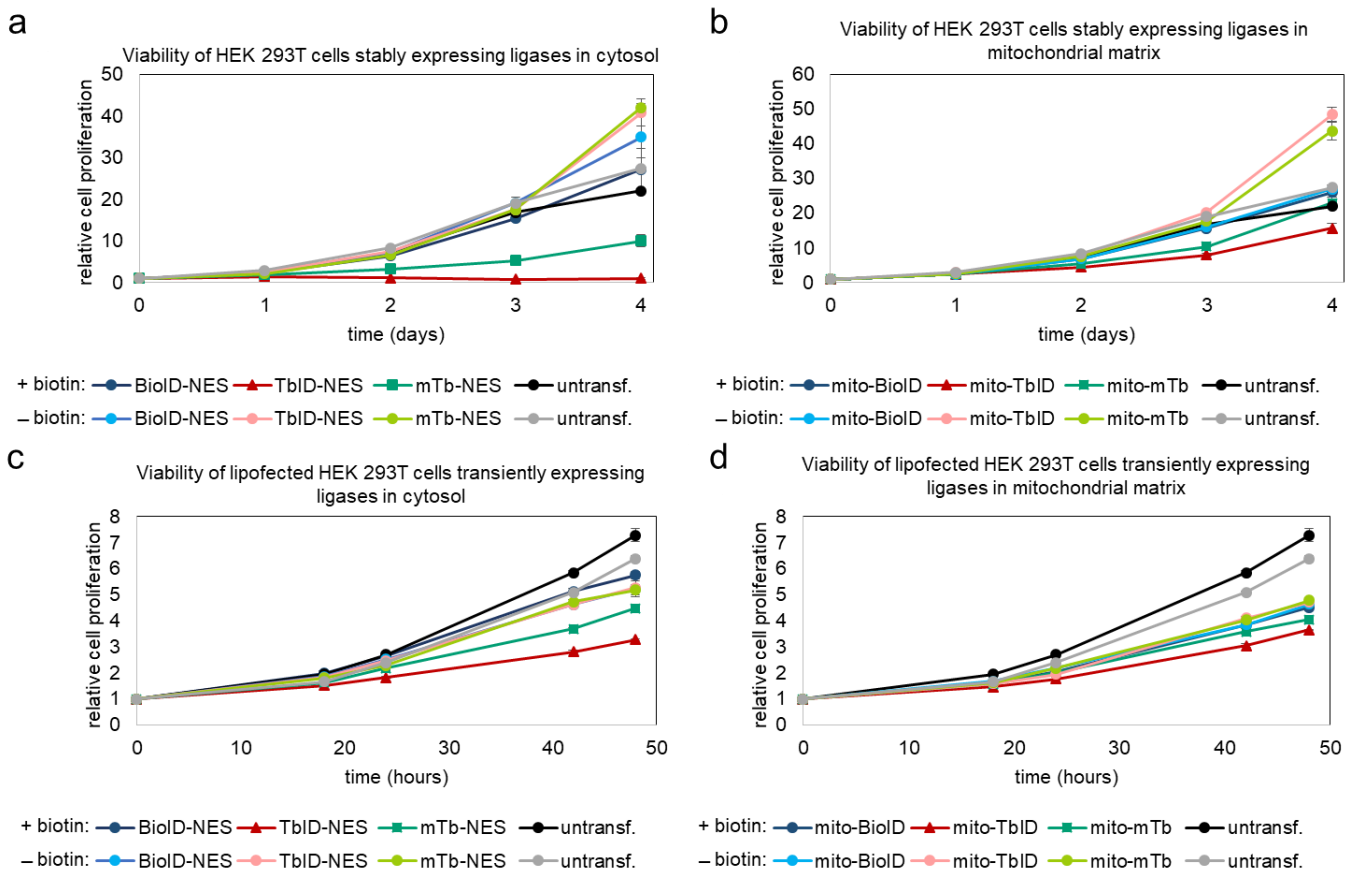

Supplementary Figure 14. Viability assays in HEK 293T cells expressing promiscuous ligase variants. (**a**–**d**) Growth curves of HEK 293T cells expressing the indicated ligases either stably (a, b) or transiently via lipofection (c, d) in the cytosol (a, c) or mitochondrial matrix (b, d). Cells, including untransfected HEK 293T controls, were plated in triplicate in matched 96-well plates. At time of plating, the indicated samples were supplemented with 50 μM exogenous biotin. At each time point, a plate was removed and processed with the Cell-Titer Glo assay (Promega) to quantify viable cells. Signal from each cell line was normalized to the initial signal at the time of plating. This experiment was performed once with three biological replicates per sample. Mean of relative cell proliferation of the three biological replicates are shown, along with error bars in s.e.m.

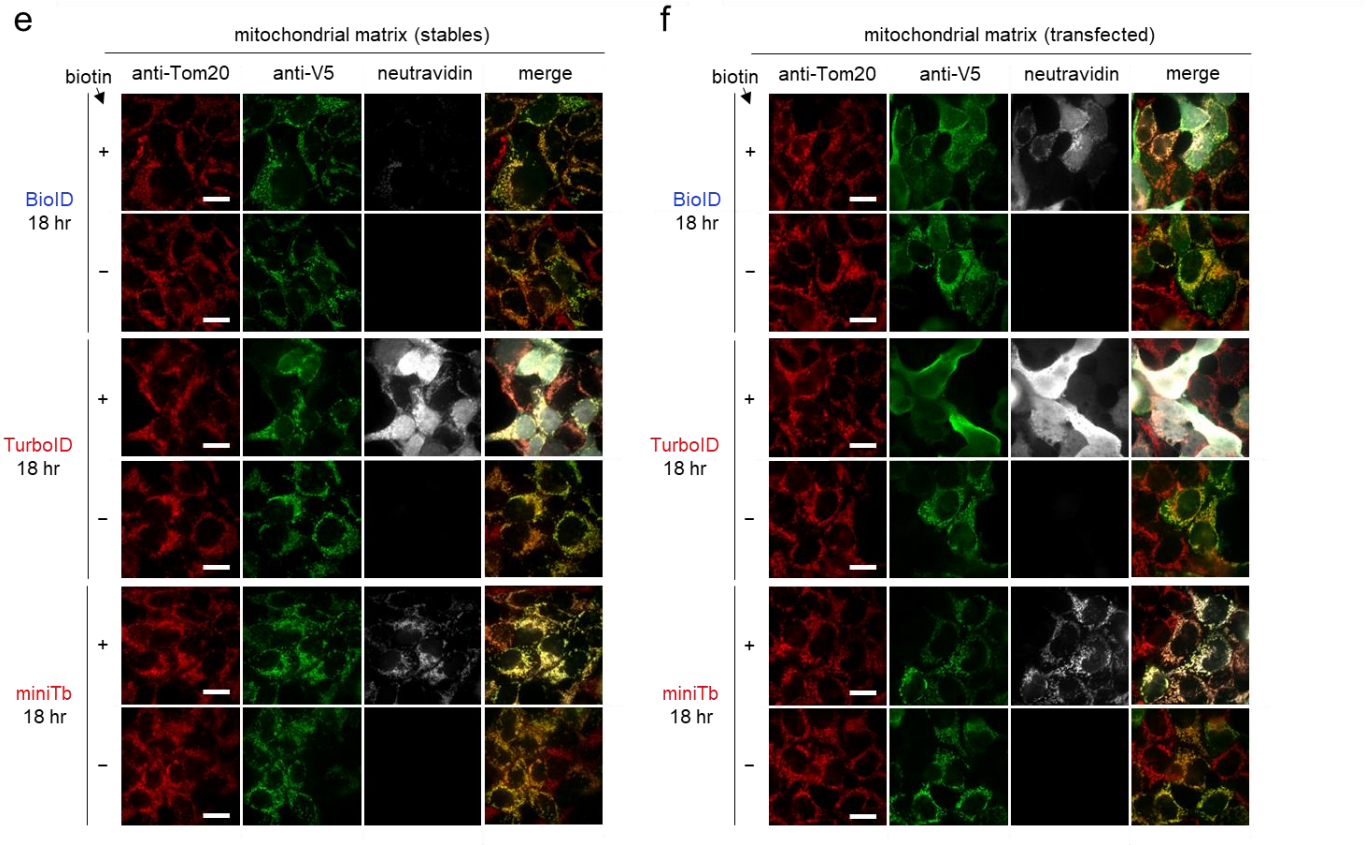

Supplementary Figure 14 (continued). Viability assays in HEK 293T cells expressing promiscuous ligase variants (continued). (**e, f**) Characterization of HEK 293T cells expressing the indicated ligases either stably (e) or transiently via lipofection (f) in the mitochondrial matrix by fluorescence microscopy. Approximately 18 hours post-transfection, cells were labeled with 50 μM exogenous biotin for 18 hours. Cells were then fixed and stained with anti-Tom20 antibody to stain mitochondria, anti-V5 to visualize ligase expression, and neutravidin-AlexFluor647 to visualize biotinylated proteins. Scale bars, 20 μm. This experiment was performed once.

a

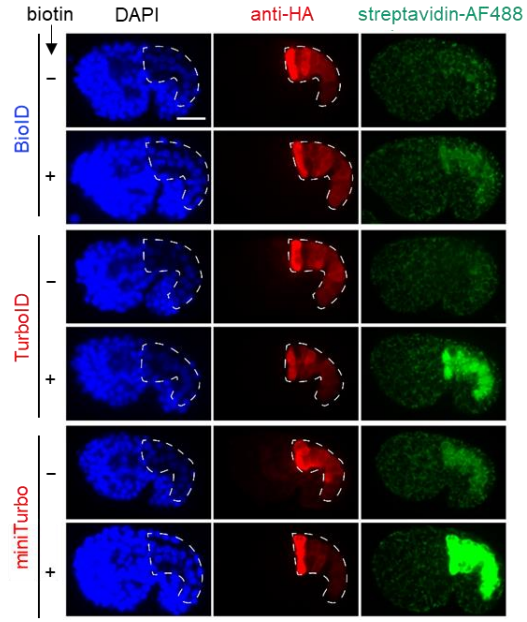

b

- biotin	BioID	TurboID	miniTurbo
stage 1 (bean)	980.7 ± 82.0	1189.5 ± 220.1	1682.4 ± 307.9
stage 2 (comma)	1089.5 ± 137.9	1013.6 ± 125.7	4190.7 ± 422.3

+ biotin	BioID	TurboID	miniTurbo
stage 1 (bean)	2362.9 ± 180.8	7144.3 ± 1254.2	13606.3 ± 1016.1
stage 2 (comma)	2931.2 ± 312.8	10493.8 ± 1283.3	19736.8 ± 1376.5

Supplementary Figure 15. Further analysis of promiscuous biotinylation in worms. (**a**) Representative images of worm embryos from **Figure 3h**, approximately 7.5 hours after the first cell cleavage (embryonic comma stage (stage 2)). Embryos were fixed and stained with streptavidin-AF488 to detect biotinylated proteins, and anti-HA antibody to detect ligase expression. Intestine is outlined by a white dotted line. Scale bar, 10 μm. Quantitation of multiple replicates shown in **Figure 3k**. (**b**) Mean values from **Figure 3k**. Number of embryos imaged (n) from top left to bottom right: 26, 18, 11, 16, 25, 8, 19, 23, 14, 14, 23, 9. Error in s.e.m.

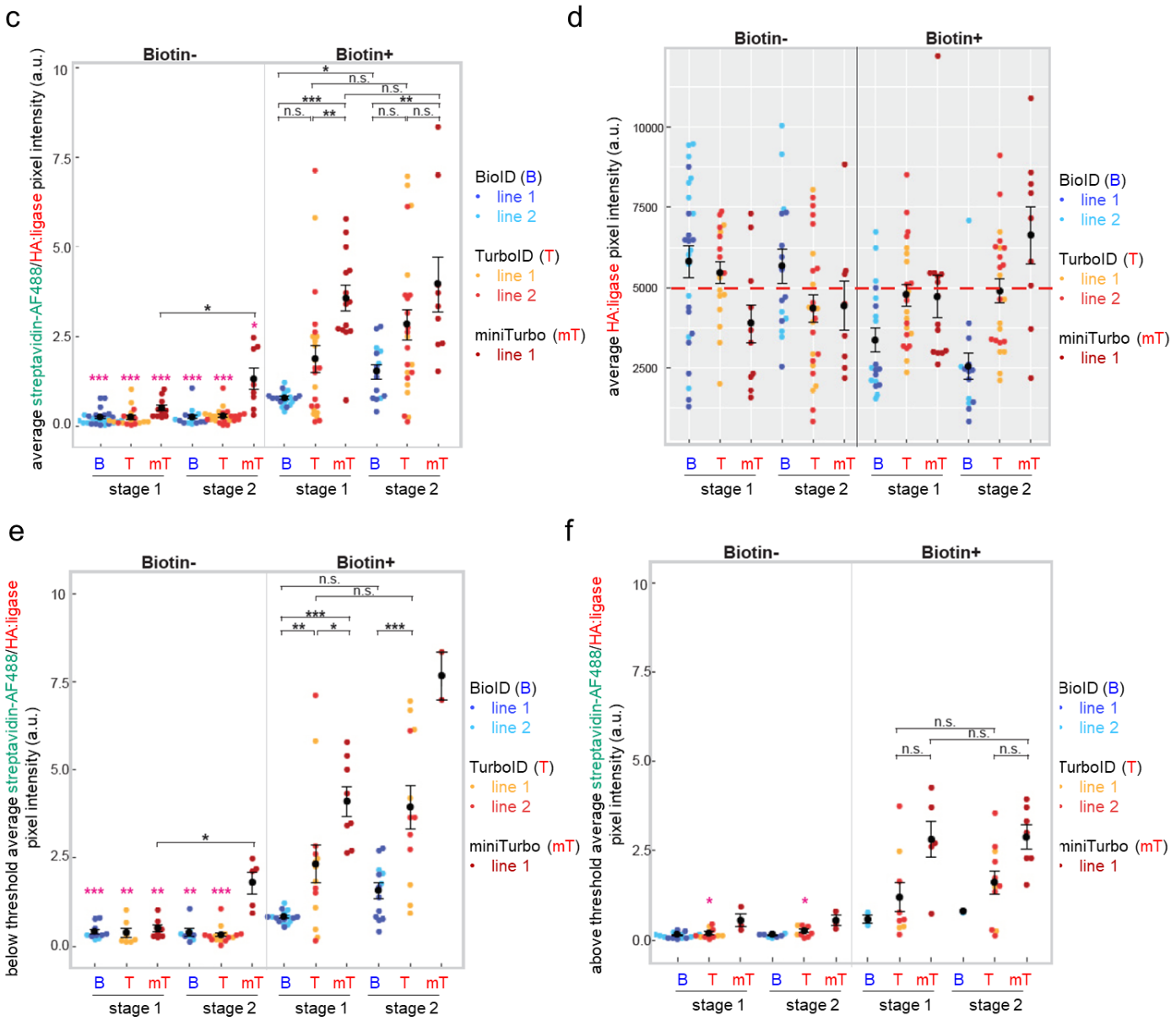

Supplementary Figure 15 (continued). Further analysis of promiscuous biotinylation in worms. (**c-f**) Saturation of apparent biotinylation levels in worms. In plots in (c) and (d), number of embryos imaged (n) from left to right: 26, 18, 11, 16, 25, 8, 19, 23, 14, 14, 23, 9. Statistical significance was determined using the Mann-Whitney U test (two-sided). ***p ≤ 0.0001, **p ≤ 0.001, *p ≤ 0.01. Pink asterisks indicate significance of pairwise comparisons between biotin- and corresponding biotin+ treated embryos. Mean is shown as a black dot for each condition, and error bars indicate s.e.m. (**c**) Ratios of streptavidin-AF488 to anti-HA:ligase mean pixel intensities for BioID (B), TurboID (T), and miniTurbo (mT) are plotted and showed similar general trends between experimental conditions compared to streptavidin-AF488 levels alone (**Figure 3k**); however, a few comparisons are no longer statistically significant. Mean values from left to right: 0.24 ± 0.04, 0.26 ± 0.06, 0.52 ± 0.08, 0.26 ± 0.06, 0.3 ± 0.04, 1.3 ± 0.3, 0.79 ± 0.04, 1.9 ± 0.37, 3.6 ± 0.36, 1.5 ± 0.20, 2.8 ± 0.43, 4.0 ± 0.76. (**d**) Mean pixel intensity of anti-HA:ligase signal is plotted for each experimental condition. We hypothesized that high expression levels of ligase might consume available biotin, thereby saturating biotinylation levels. Thus, we binned the data into two groups marked by the red dotted line: "low" HA signal was defined as HA values below the line and "high" HA signal was defined as values above the line. After binning, some groups contained fewer than five data points, for which we did not run statistical analyses. Streptavidin-AF488 to anti-HA:ligase mean pixel intensity ratios for low- (c) and high- (d) HA expressing embryos were plotted separately. (**e**) When we considered only embryos that have "low" HA levels, differences between most groups were significant. (**f**) In contrast, when we considered only embryos that have "high" HA levels, differences between several groups were no longer significant.

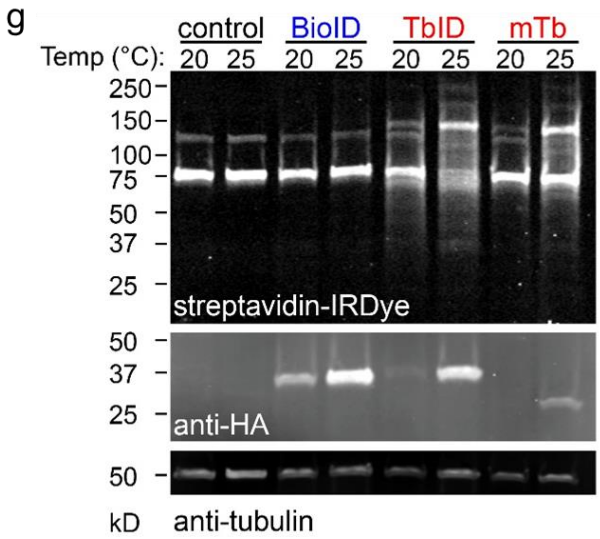

Supplementary Figure 15 (continued). Further analysis of promiscuous biotinylation in worms. (**g**) Higher temperatures increase biotinylation extent in worms. Worms either maintained at 20°C or grown at 25°C for one generation were collected for analysis at the same developmental time (newly gravid hermaphrodites). The same number of lysed worms was loaded per lane and protein levels were similar (see anti-tubulin blot). BioID, Turbo ID, and miniTurbo were all expressed at higher levels at 25°C than at 20°C. Similarly, worms expressing TurboID and miniTurbo also had increased biotinylation at 25°C. Despite increased BioID expression levels at 25°C, we never observed increased biotinylation. This experiment was performed three times with similar results.

a

Bacteria	Experimental Condition		Transgene[1]	Viable (%)	Delayed development (%)[2]	Transgene positive (%)[3]	Replicates
Biotin+	BioID	Line 1	+	100 ± 0	11.5 ± 7.3	83.4	5
			–	93.0 ± 12.4	4.9 ± 4.7	N/A	5
		Line 2	+	98.5 ± 2.9	8.2 ± 6.9	70.9	4
			–	100 ± 0	3.6 ± 4.7	N/A	4
	TurboID	Line 1	+	98.5 ± 2.9	22.4 ± 4.4	59.2	4
			–	89.2 ± 16.8	6.9 ± 7.5	N/A	5
		Line 2	+	92.5 ± 20.7	26.6 ± 27.3	61.7	5
			–	88.7 ± 16.0	7.0 ± 6.8	N/A	5
Biotin-	BioID	Line 1	+	84.5 ± 19.0	7.0 ± 5.2	68.8	5
			–	76.9 ±13.9	1.5 ± 2.1	N/A	5
		Line 2	+	92.8 ± 9.1	4.6 ± 5.9	77.6	5
			–	94.1 ± 5.1	0.93 ± 1.9	N/A	4
	TurboID	Line 1	+	91.6 ± 14.8	9.1 ± 3.1	61.7	5
			–	98.7 ± 2.9	1.1 ± 2.4	N/A	5
		Line 2	+	88.1 ± 9.4	3.3 ± 4.5	55.5	5
			–	87.7 ± 14.3	6.9 ± 9.7	N/A	5

Supplementary Figure 16. Effect of promiscuous ligase variants on *C. elegans* viability and development. Worm strains were raised on either biotin+ (OP50) or biotin- (MG1655bioB:kan) *E. coli*. (**a**) Table summarizing viability and development data compiled for two independent lines of worms expressing BioID or TurboID. Each experimental condition was performed with the indicated number of replicates. Averages and standard deviation between replicates are shown. 1) For each indicated experimental condition, an adult worm expressing a ligase transgene from an extrachromosomal array (+) or a sibling lacking a transgene (–, control) was laid on a plate and allowed to lay eggs for 4 hours. 2) After three days, worm progeny were scored as either gravid adult or developmentally delayed, a category that includes larval stages and adults without embryos. 3) The percent of worm progeny expressing the indicated transgene was calculated.

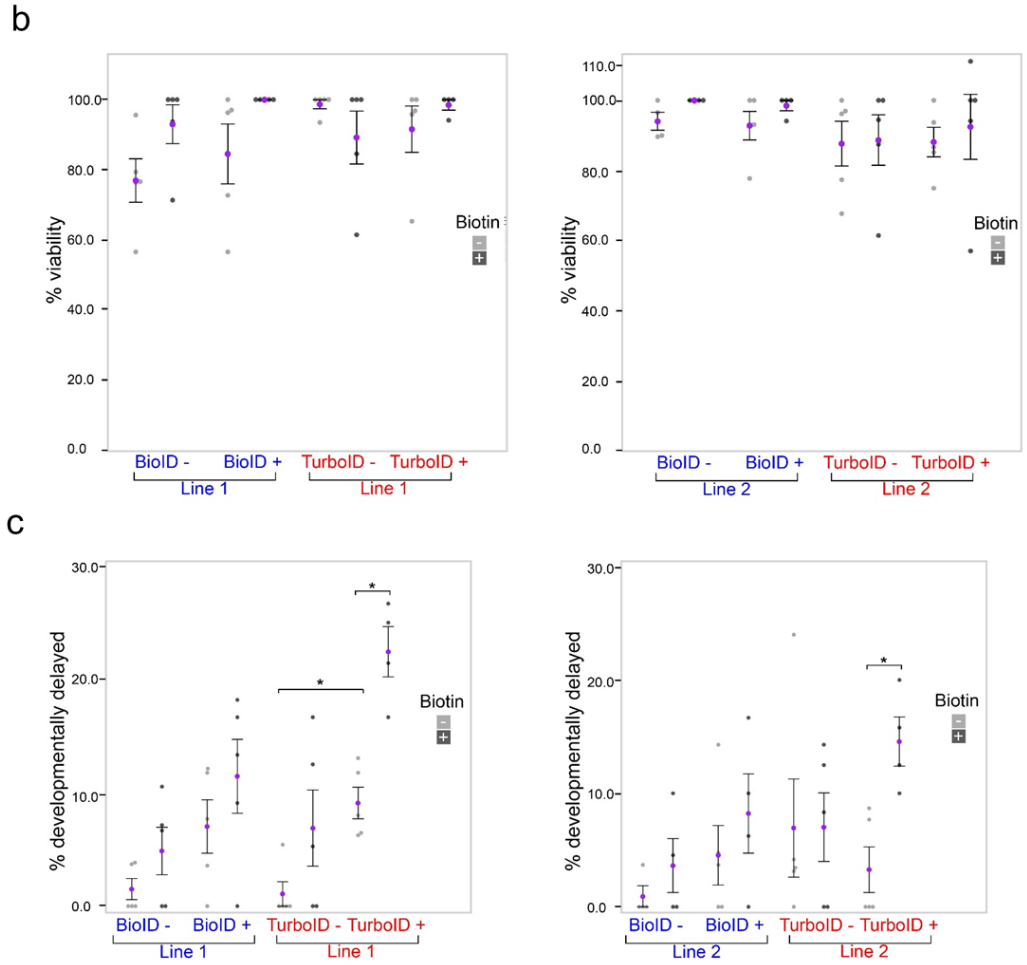

Supplementary Figure 16 (continued). Effect of promiscuous ligase variants on *C. elegans* viability and development. Worm strains were raised on either biotin+ (OP50) or biotin- (MG1655bioB:kan) *E. coli*. Dot plots showing (**b**) percent viability and (**c**) percent developmental delay of worms expressing BioID or TurboID or their sibling array negative worms in either biotin+ or biotin- conditions. No statistical difference in viability was detected with expression of the ligase variants or with the addition of biotin for BioID (Lines 1 and 2) and TurboID (Lines 1 and 2). No statistical difference in developmental timing was detected with expression of BioID (Lines 1 and 2) or with the addition of biotin. However, for the comparisons indicated, statistically significant developmental delays were detected with expression of TurboID (Lines 1 and 2). Statistical significance was determined using the Mann-Whitney U test. In these plots, comparisons indicated with a * have a p value of 0.01. Each dot represents one biological replicate. Light gray dot signifies biotin- condition and dark gray dot signifies biotin+ condition. Purple dot is the mean, and error bars are s.e.m.

Supplementary Table 1. Mutations in TurboID, miniTurbo, BioID and key intermediate clones.

Mutant	amino acids	K2	Q65	I87	R118	E140	Q141	A146	S150	L151	M157	V160	T192	K194	M209	M241	S263	L298	I305	E313
BioID	1-321				R118G			A146Δ												
BirA-R118S	1-321				R118S			A146Δ												
R6-1	1-321	K2E			R118S			A146Δ			M157T							L298P		
R6-2	1-321		Q65P		R118S			A146Δ		L151P									I305V	E313K
G1	1-321		Q65P		R118S			A146Δ		L151P									I305V	
G2	1-321		Q65P		R118S			A146Δ	S150G	L151P			T192A						I305V	
G3	1-321		Q65P	I87V	R118S	E140K	Q141R	A146Δ	S150G	L151P		V160A	T192A		M209V				I305V	
G3Δ	64-321		Q65P	I87V	R118S	E140K	Q141R	A146Δ	S150G	L151P		V160A	T192A		M209V				I305V	
miniTurbo	64-321		Q65P	I87V	R118S	E140K	Q141R	A146Δ	S150G	L151P		V160A	T192A	K194I	M209V				I305V	
TurboID	1-321		Q65P	I87V	R118S	E140K	Q141R	A146Δ	S150G	L151P		V160A	T192A	K194I	M209V	M241T	S263P		I305V	

Supplementary Table 2. True positive and false positive lists used to filter and analyze ERM datasets.

Tab 1. True positive list of 90 well-established ERM proteins. Manually curated from literature[5]. Used to determine TMT ratio cutoffs in **Supplementary Figures 9d, e**, and to calculate ERM proteome coverage (**Supplementary Figure 9f**).

Tab 2. False positive list of 173 soluble mitochondrial matrix proteins[6]. Used to determine TMT ratio cutoffs against untransfected control in **Supplementary Figures 9d, e**.

Tab 3. False positive list of 7421 proteins with non-secretory annotation in GOCC[3,4]. Used to determine TMT ratio cutoffs against cytosolic reference controls in **Supplementary Figures 9d, e**.

Tab 4. True positive list of 11,838 proteins with secretory annotation in GOCC[3,4], Human Protein Atlas[7], Human Plasma Proteome Database[8], or literature. Used to calculate ERM proteome specificity in **Figure 2e**.

Tab 5. List of 5387 proteins classified by ER, Golgi apparatus, or plasma membrane annotation in GOCC[3,4]. Used to calculate subsecretory proteome specificity **Figure 2f**.

Tab 6. List of 237 classified by ER transmembrane, ER soluble and cytosol-facing, or ER soluble and luminal annotation according to GOCC, TMHMM, Uniprot, or literature. Used to calculate ER proteome specificity **Figure 2g**.

Tab 7. List of 2437 proteins with cytosolic annotation in GOCC that lack annotated or predicted transmembrane domains according to UniProt or TMHMM[5]. Used for scatter plot analyses in **Supplementary Figure 9e**.

Tab 8. Column definitions.

Supplementary Table 3. True positive and false positive lists used to filter and analyze nuclear proteomic datasets.

Tab 1. True positive list of 6710 proteins with nuclear annotation in GOCC[3,4]. Used to determine TMT ratio cutoffs in **Supplementary Figure 10h**, and also to calculate nuclear proteome specificity (**Figure 2h**).

Tab 2. False positive list of 6815 proteins with non-nuclear annotation in GOCC[3,4]. Used to determine TMT ratio cutoffs in **Supplementary Figure 10h**.

Tab 3. True positive list of 230 well-established nuclear proteins. Curated from Human Protein Atlas[7]. Used to calculate nuclear proteome coverage (**Supplementary Figure 10j**).

Tab 4. Column definitions

Supplementary Table 4. True positive and false positive lists used to filter and analyze mitochondrial matrix proteomic datasets.

Tab 1. True positive list of 1555 proteins with mitochondrial annotation in GOCC[3,4] Used to determine TMT ratio cutoffs in **Supplementary Figure 10i**, and also to calculate mitochondrial proteome specificity (**Figure 2h**).

Tab 2. False positive list of 2410 proteins with non-mitochondrial annotation[9]. Used to determine TMT ratio cutoffs in **Supplementary Figure 10i.**

Tab 3. True positive list of 173 well-established mitochondrial matrix proteins curated from previous proteomes and literature[6]. Used to calculate mitochondrial matrix proteome coverage (**Supplementary Figure 10j**).

Tab 4. Column definitions.

Supplementary Table 5. ER membrane (ERM) proteomic data.

Tab 1. ERM proteome from BioID 18 hour labeling. 707 proteins ranked by Replicate 1 ERM-BioID/untransfected enrichment ratio (127N/126C TMT ratio).

Tab 2. ERM proteome from TurboID 10 minute labeling. 808 proteins ranked by Replicate 1 ERM-TurboID (10 min)/untransfected enrichment ratio (129N/126C TMT ratio).

Tab 3. ERM proteome from TurboID 1 hour labeling. 1180 proteins ranked by Replicate 1 ERM-TurboID (1 hr)/untransfected enrichment ratio (130N/126C TMT ratio).

Tab 4. Overlap of proteins detected in BioID, TurboID 10 minute, and TurboID 1 hour ERM proteomes. Used to generate Venn diagram in **Supplementary Figure 9g**.

Tab 5. "-Biotin" ERM proteome from TurboID omit biotin sample. 840 proteins ranked by Replicate 1 ERM-TurboID (omit biotin)/untransfected enrichment ratio (131C/126C TMT ratio).

Tab 6. Complete mass spectrometry data from ERM proteomic experiment. All proteins with 2 or more quantified, unique peptides are listed. TMT ratios are normalized as described in the Methods.

Tab 7. Column definitions.

Supplementary Table 6. Nuclear proteomic data.

Tab 1. Nuclear proteome BioID 18 hour labeling. 1512 proteins ranked by Replicate 1 BioID-NLS/biotin omitted enrichment ratio (126/127 TMT ratio).

Tab 2. Nuclear proteome from TurboID 10 minute labeling. 1455 proteins ranked by Replicate 1 TurboID-NLS/ biotin omitted enrichment ratio (128/129 TMT ratio).

Tab 3. Nuclear proteome from miniTurbo 10 minute labeling. 1362 proteins ranked by Replicate 1 miniTurbo-NLS/ biotin omitted enrichment ratio (130/131 TMT ratio).

Tab 4. Overlap of proteins detected in BioID, TurboID, and miniTurbo nuclear proteomes. Used to generate Venn diagram shown in **Supplementary Figure 10k**.

Tab 5. "-Biotin" nuclear proteome from TurboID omit biotin sample. 993 proteins ranked by Replicate 1 TurboID-NLS omit biotin/BioID-NLS omit biotin enrichment ratio (129/127 TMT ratio).

Tab 6. Complete mass spectrometry data from nuclear proteomic experiment. All proteins with 2 or more quantified, unique peptides are listed. TMT ratios are normalized as described in the Methods.

Tab 7. Column definitions

Supplementary Table 7. Mitochondrial matrix proteomic data.

Tab 1. Mitochondrial matrix proteome from BioID 18 hour labeling. 362 proteins ranked by Replicate 1 mito-BioID/biotin omitted enrichment ratio (126/127 TMT ratio).

Tab 2. Mitochondrial matrix proteome from TurboID 10 minute labeling. 314 proteins ranked by Replicate 1 mito-TurboID/ biotin omitted enrichment ratio (128/129 TMT ratio).

Tab 3. Mitochondrial matrix proteome from miniTurbo 10 minute labeling. 359 proteins ranked by Replicate 1 mito-miniTurbo/ biotin omitted enrichment ratio (130/131 TMT ratio).

Tab 4. Overlap of proteins detected in BioID, TurboID, and miniTurbo mitochondrial matrix proteomes. Used to generate Venn diagram shown in **Supplementary Figure 10k**.

Tab 5. "-Biotin" mitochondrial matrix proteome from TurboID omit biotin sample. 1540 proteins ranked by Replicate 1 mito-TurboID omit biotin/mito-BioID omit biotin enrichment ratio (129/127 TMT ratio).

Tab 6. Complete mass spectrometry data from mitochondrial matrix proteomic experiment. All proteins with 2 or more quantified, unique peptides are listed. TMT ratios are normalized as described in the Methods.

Tab 7. Column definitions.

Supplementary Table 8. Table of plasmids used in this study.

Plasmid name	Plasmid vector	Promoter	Expression in	Features	Variants	Details	Used for	Used in
P1 - P8	pCDNA3	CMV	mammalian	NotI-myc-NheI-BirA-NES-Stop-XhoI	BirA (R118G) (= BioID); BirA (R118S); BirA (R118T); BirA (R118C); BirA (R118N); BirA (R118V); BirA (R118P); BirA (R118K)	myc: EQKLISEEDL; NES: LQLPPLERLTLD[10]	transient mammalian cytosol expression	Supplementary Fig. 1, 2
P9 - P17	pCTCON2	GAL1	yeast	EcoRI-Aga2P-HA-TEVs-15aa linker-NheI-BirA-BamHI-myc-Stop-XhoI	BirA (R118S); R6-1; R6-2; G1; G2; G3; G3Δ; miniTurbo; TurboID (see Supplementary Table 1)	TEVs: ENLYFQG, cleavage recognition site for TEV protease, which was not employed in this study; 15aa linker: GGGGSGGGGSGGGGS; myc: EQKLISEEDL	inducible yeast cell surface expression for yeast display directed evolution	Fig. 1c, e; Supplementary Fig. 3, 4
P18 - P27	pCDNA3	CMV	mammalian	NotI-V5-NheI-BirA-NES-Stop-XhoI	BirA (R118S); G1; G2; G3; G3Δ; miniTurbo; TurboID; BioID (see Supplementary Table 1); A. aeolicus BirA (R40G) (=BioID2); B. Subitilis BirA (R124G) (=BASU)	V5: GKPIPNPLLGLDST; NES: LQLPPLERLTLD[10]	transient mammalian cytosol expression	Fig. 1f, g; Fig. 2a ,b; Supplementary Fig. 2, 4, 5, 6, 7, 14
P28	pDisplay	CMV	mammalian	EcoRI-Ig K-chain ss-HA-BglII-BirA-myc-TM-Stop-NotI	BioID; TurboID, miniTurbo (see Table 2-1)	Ig K-chain ss: METDTLLLWVLLLWVPGSTGD; HA: YPYDVPDYA; myc: EQKLISEEDL; TM: transmembrane domain of PDGF receptor from pDisplay (Invitrogen)	transient mammalian cell surface expression	Supplementary Fig. 5
P29 - P31	pCDNA3	CMV	mammalian	NotI-V5-NheI-BirA-EcoRI-3aa linker-NLS-Stop-XhoI	BioID; TurboID, miniTurbo (see Supplementary Table 1)	V5: GKPIPNPLLGLDST; 3aa linker: SRA; NLS: DPKKKRKVDPKKKRKVDPKKKRKV[11]	transient mammalian nucleus expression	Fig. 2c, h; Supplementary Fig. 10a, b, d, f, h, j, k; Supplementary Fig. 11
P32 - P34	pLX304	CMV	mammalian	attB1-BstBI-mito-BamHI-BirA-NheI-V5-Stop-attB2-NheI-AgeI	BioID; TurboID, miniTurbo (see Supplementary Table 1)	mito (mitochondrial matrix targeting sequence from COX4): MLATRVFSLVGKRAISTSVCVRAH[12]; V5: GKPIPNPLLGLDST	stable mammalian mitochondrial matrix expression	Fig. 2c, h; Supplementary Fig. 10a, c, e, g, i, j, k; Supplementary Fig. 11, 14
P35	pVSVG					lentiviral envelope plasmid	producing lentivirus (for P33 - P35)	Fig. 2c, d, e, f, g, h; Supplementary Fig. 8, 9; Supplementary Fig. 10a, c, e, g, i, j, k;
P36	Δ8.9					lentiviral helper plasmid	producing lentivirus (for P33 - P35)	Fig. 2c,d, e, f; Supplementary Fig. 8, 9, 10a, c, e, g, i, j, k;
P37 - P39	pCDNA3	CMV	mammalian	HindIII-C1(1-27)-4aa linker-NotI-19aa linker-BirA-NheI-V5-Stop-BamHI	BioID; TurboID, miniTurbo (see Supplementary Table 1)	C1(1-27) (endoplasmic reticulum membrane anchor derived from cytochrome P450): MDPVVVLGLCLSCLLLLSLWKQSYGGG[13]; 4aa linker: GSGS; 19aa linker: GSGSGSGSGSGSGSGSGSG; V5: GKPIPNPLLGLDST	transient mammalian ER membrane expression (cytosol facing)	Fig. 2c
P40 - P42	pDisplay	CMV	mammalian	EcoRI-Ig K-chain ss-HA-BglII-BirA-NheI-V5-KDEL-Stop-NotI	BioID; TurboID, miniTurbo (see Supplementary Table 1)	Ig K-chain ss: METDTLLLWVLLLWVPGSTGD; HA: YPYDVPDYA; V5: GKPIPNPLLGLDST; ER localization sequence: KDEL[14]	transient mammalian ER lumen expression	Fig. 2c

P43 - P45	pLX304	CMV	mammalian	attB1-BstBI-V5-NheI-BirA-EcoRI-MAVS(510-540)-Stop-attB2-NheI-AgeI	BioID; TurboID, miniTurbo (see Supplementary Table 1)	V5: GKPIPNPLLGLDST; MAVS(510-540) (outer mitochondrial membrane anchor derived from mitochondrial antiviral signaling protein): RPSPGALWLQVAVTGVLVVT LLVVLYRRRLH[15]	stable mammalian outer mitochodrial membrane expression	Supplementary Fig. 8
P46 - P48	pLX304	CMV	mammalian	attB1-BstBI-C1(1-27)-4aa linker-NotI-19aa linker-BirA-NheI-V5-Stop-attB2-NheI-AgeI	BioID; TurboID, miniTurbo (see Supplementary Table 1)	C1(1-27) (endoplasmic reticulum membrane anchor derived from cytochrome P450): MDPVVVLGLCLSCLLLLSLWKQSYGGG[13]; 4aa linker: GSGS; 19aa linker: GSGSGSGSGSGSGSGSGSG; V5: GKPIPNPLLGLDST	stable mammalian ER membrane expression	Fig. 2d, e, f, g; Supplementary Fig. 8, 9
P49 – P50	pLX304	CMV	mammalian	attB1-BstBI-V5-NheI-BirA-NES-Stop-attB2-NheI-AgeI	BioID; TurboID (see Supplementary Table 1)	V5: GKPIPNPLLGLDST; NES: LQLPPLERLTLD[10]	stable mammalian cytosol expression	Fig. 2d, e, f, g; Supplementary Fig. 9, 14
P51 - P53	pRS415	GAL1	yeast	BamHI-BirA-NheI-V5-Stop-XhoI	BioID; TurboID, miniTurbo (see Supplementary Table 1)	V5: GKPIPNPLLGLDST	inducible yeast cytosol expression	Fig. 3a
P54 - P56	pYFJ16	T5	bacteria	EcoRI-His6-MBP-4aa linker-AgeI-5 aa linker-BirA-Stop-AscI	BioID; TurboID, miniTurbo (see Supplementary Table 1)	His6: HHHHHH; MBP: maltose binding protein; 4aa linker: GGGS; 5aa linker: GGSSG	Inducible bacterial cytosol expression	Fig. 3b
P57 - P59	pEntr			attL1-V5-NheI-BirA-stop-attL2	BioID; TurboID, miniTurbo (see Supplementary Table 1)	V5: GKPIPNPLLGLDST, Thermo Fisher	Entry vector for Gateway LR recombination into destination vector	
P60 - P62	pWalium-roe	UAS	D. melanogaster	attB1-V5-NheI-BirA-stop-attB2, white+, attB	BioID; TurboID, miniTurbo (see Supplementary Table 1)	V5: GKPIPNPLLGLDST, REF PMID: 26320097	Generating trasngenic flies for Gal4-inducible expression	Fig.3d, e, g; Supplementary Fig. 12, 13
P63	pCDNA3	CMV	mammalian	NotI-mito-BamHI-BirA-NheI-V5-Stop-XhoI	BioID; TurboID, miniTurbo (see Supplementary Table 1)	mito (mitochondrial matrix targeting sequence from COX4): MLATRVFSLVGKRAISTSVCVRAH[12]; V5: GKPIPNPLLGLDST	Transient mammalian mitochondrial matrix expression	Supplementary Fig. 14
pAS28	pJF241 (which contains Bluescript backbone)	ges-1	C. elegans	Asc1-ges-1p-Fse1-3xHA-BirA-Xma1-unc54-Xho1	BioID	3xHA: YPYDVPDYAYPYDVPDYAYP YDVPDYA	Intestinal expression of BioID	Fig. 3h-k, Supplementary Fig. 15, 16
pAS31	pJF241 (which contains Bluescript backbone)	ges-1	C. elegans	Asc1-ges-1p-Fse1-3xHA-BirA-Xma1-unc54-Xho1	TurboID	3xHA: YPYDVPDYAYPYDVPDYAYP YDVPDYA	Intestinal expression of TurboID	Fig. 3h-k, Supplementary Fig. 15, 16
pAS32	pJF241 (which contains Bluescript backbone)	ges-1	C. elegans	Asc1-ges-1p-Fse1-3xHA-BirA-Xma1-unc54-Xho1	miniTurbo	3xHA: YPYDVPDYAYPYDVPDYAYP YDVPDYA	Intestinal expression of miniTurbo	Fig. 3h-k, Supplementary Fig. 15, 16

Supplementary Table 9. Table of antibodies used in this study.

antibody	source	vendor	catalog number	dilutions used
anti-myc	mouse	Calbiochem	OP10	Western blotting: 1:1000
anti-mouse-HRP	goat	BioRad	170-6516	Western blotting: match dilution of primary antibody used
anti-myc	chicken	Invitrogen	A-21281	yeast surface immunostaining: 1:400
anti-chicken-AlexaFluor647	goat	Invitrogen	A-21449	yeast surface immunostaining: 1:200
streptavidin-R-phycoerythrin	--	Jackson Immunoresearch	016-110-084	yeast surface immunostaining: 1:100
anti-biotin	rabbit	ImmuneChem	ICP0611	yeast surface immunostaining: 1:50
anti-rabbit-R-phycoerythrin	goat	Life Technologies	P-2771MP	yeast surface immunostaining: 1:50
streptavidin-HRP	--	Invitrogen	S911	Western blotting: 1:3000; TSA on yeast surface: 1:200
anti-V5	mouse	Invitrogen	46-0705	Western blotting: 1:10,000; mammailain cell immunostaining: 1:2000
anti-calreticulin	mouse	Calbiochem	208912	Western blotting: 1:1000
anti-BCAP31	rabbit	Proteintech	11200-1-AP	Western blotting: 1:500
anti-Tom70	rabbit	Proteintech	14528-1-AP	Western blotting: 1:500
anti-Tom20	mouse	Santa Cruz Biotecnology	sc-17764	Western blotting: 1:500
anti-HXK I	mouse	Santa Cruz Biotecnology	sc-46695	Western blotting: 1:100
anti-NDUFS6	rabbit	Abcam	ab195808	Western blotting: 1:2000
anti-calnexin	rabbit	Santa Cruz Biotecnology	sc-11397	Western blotting: 1:50
DAPI	--			mammalian cell immunostaing: 1:1000
anti-Tom20	rabbit	Santa Cruz Biotecnology	sc-11415	mammalian cell immunostaing: 1:500
anti-rabbit-AlexaFluor568	goat	Invitrogen	A-11011	mammalian cell immunostaing: 1:1000
neutravidin-AlexaFluor647	--	Life Techologies (homemade)	neutravidin: A-2666; AlexaFluor647-NHS: A20006	mammalian cell immunostaing: 1:1000
anti-His6	mouse	Calbiochem	OB05	Western blotting: 1:200
anti-mouse Alexa 647	goat	Invitrogen	A-21236	*Drosophila* cell immunostaining: 1:500
anti-mouse Alexa 800	goat	Invitrogen	A32730	*Drosophila* western blotting: 1:5000

DAPI	--	Sigma		*C. elegans* immunostaining 1:10000
anti-HA	mouse	Abcam	ab130275	*C. elegans* immunostaining 1:100
Streptavidin-AF488	--	Thermo Fisher Scientific	S32354	*C. elegans* immunostaining 1:200
CY3-anti-mouse	goat	Jackson Immunoresearch Laboratories	115-165-166	*C. elegans* immunostaining 1:200
anti-alpha tubulin	rat	Abcam	ab6161	*C. elegans* Western blotting (1:5000)
anti-HA	rat	Roche	11867423001	*C. elegans* Western blotting (1:5000)
anti-rat IRDye 680RD	goat	LI-COR	925-68076	*C. elegans* Western blotting (1:5000)
Streptavidin-IRDye 800CW	--	LI-COR	925-32230	*C. elegans* Western blotting (1:5000)

Supplementary Note 1: Further details on the directed evolution of TurboID and miniTurbo

To engineer a more catalytically active variant of promiscuous *E. coli* biotin ligase (BirA), we first examined the crystal structure of wild-type BirA[16–18] to rationally select residues to mutagenize. Two disordered loops near the BirA active site become ordered upon biotin binding (residues 115-125) and ATP binding (residues 212-221)[17,19]. Upon ordering, these loops surround biotin and ATP, partially enclosing the active site and forming several stabilizing interactions that facilitate the synthesis of biotin-5'-AMP. The R118G mutation that imparts promiscuity in BioID resides in the biotin binding loop[20,21]. Removal of this arginine weakens the enzyme's affinity for biotin and biotin-5'-AMP[22], likely opening the active site and allowing biotin-5'-AMP to diffuse away from the enzyme. While this property allows promiscuous labeling of surrounding proteins, the extreme arginine to glycine mutation significantly compromises the efficiency of biotin-5'-AMP synthesis[22]. In an attempt to weaken the enzyme's affinity for biotin-5'-AMP while minimizing negative impact on activity, we mutated several residues in both the biotin binding loop and ATP binding loop, including several residues at the R118 position: R118A, R118S, R118T, R118C, R118N, R118V, R118P, R118K, R118G + G115A, R119A, R121A, R121S, R121G, K122A, R212A, R213A, V214A, V218A, V219A (data not shown). None of the point mutations at residues other than R118 imparted promiscuous activity to wild-type BirA, and all but one of the point mutations at R118 abrogated or reduced promiscuous activity relative to R118G. Only one mutation, R118S, showed modestly higher promiscuous activity than BioID (R118G) (**Supplementary figure 1**). Because rational design did not appear to be a promising path to engineering a more catalytically active promiscuous biotin ligase, we decided to perform directed evolution using BirA-R118S as our template.

We used yeast display as our platform for directed evolution. We fused BirA-R118S or a library of R118S-derived mutants (generated by error prone PCR) to the yeast cell surface mating protein Aga2p. We incubated the yeast cells with biotin and ATP for 18 hours to enable ligase-catalyzed proximity labeling (PL) to occur on the surface of each cell. Yeast were labeled at such a dilution that trans-labeling across yeast cells was negligible. We then stained the cells with streptavidin-phycoerythrin to visualize biotinylation sites, and anti-myc antibody to quantify ligase expression level, before two dimensional FACS sorting as shown in **Figure 1b**. **Figure 1c** shows that biotinylation activity was undetectable by FACS for both BirA-R118S and our mutant library on the yeast surface, even with a labeling time of 18 hours. We could not proceed with a selection if none of the clones in our library showed activity above background. To increase the sensitivity of our assay, we explored amplification of biotin signal using the "tyramide signal amplification (TSA)" approach[2]. Instead of directly staining for biotinylation sites on the yeast surface with streptavidin-phycoerythrin, we first stained with streptavidin-horseradish peroxidase conjugate, then reacted with biotin-phenol to create more biotinylation sites[2,6], and finally stained with streptavidin-phycoerythrin (**Supplementary Figure 3b**). This approach made it possible to detect a small amount of signal over background (**Figure 1c**), and allowed us to begin directed evolution. We performed our first four rounds of selection using the TSA protocol[2], and reduced the labeling time gradually from 18 hours to 6 hours. After round four, activity of the pool was sufficient to omit the TSA[2] step, and we again decreased our biotin labeling time from 3 hours to 1 hour (**Supplementary Figure 3b**).

Characterization of enriched BirA mutants after six rounds of selection revealed that we had enriched some with high self-biotinylation activity. For example, clone R6-2 contains an E313K mutation that points directly into the BirA active site. We used mutagenesis to remove this lysine, and found that the resulting mutant, now called "G1", still had ~8-fold greater promiscuous biotinylation activity than our starting template, BirA-R118S (**Supplementary Figure 3b**). Hence we used G1, together with another clone, R6-1, as starting templates for a second library, to be input into a second generation of directed evolution. This time, to avoid enriching mutants with strong self-biotinylation, we treated the yeast, in some rounds of selection, with the reducing agent TCEP prior to streptavidin and myc staining, in order to cleave the Aga1p-Aga2p disulfide bonds that retain ligase clones on the yeast surface (**Supplementary Figure 3c**). Six rounds of selection produced clone G2, with six mutations, as our best ligase mutant (**Supplementary Figure 3c**; see **Methods** for additional details on selection conditions, and **Supplementary Table 1** for sequences G1, G2, and other key clones).

We continued with a third generation of directed evolution, using G2 as a template to create a new library of mutants. Over four rounds of selection, biotin labeling time was reduced from 1 hour to 10 minutes. The resulting winner, G3, was ~17-fold more active than our starting template, BirA-R118S, but we noticed considerable activity on the yeast surface even without exogenous biotin added (**Supplementary Figure 3d**). This suggests that G3 had evolved higher affinity for biotin and was able to utilize the low levels of biotin present in yeast culture media. An experiment in biotin-depleted media confirmed this hypothesis (**Supplementary Figure 3e**). We recognized the importance of remedying this problem because a BirA mutant that is capable of biotinylating prior to exogenous biotin addition prevents precise temporal control over the PL reaction. Starting from G3, we took two divergent paths.

For one path, we implemented a fourth generation of directed evolution, starting from a G3 mutant with its N-terminal domain (residues 1-63) deleted ("G3Δ"). **Supplementary Figure 3e** shows that this deletion alone reduces G3's affinity for biotin, consistent with previous studies[23]. We conducted seven rounds of selection, including negative selections in which exogenous biotin was withheld (**Supplementary Figure 3f**). The result was miniTurbo, with 13 mutations relative to wild-type BirA (**Supplementary Figure 3g** and **Figure 1d**).

In a second path, we performed a series of positive and negative selections on a library derived from full-length G3 (**Supplementary Figure 3h**). One evolved mutation was retained, and we also carried over two mutations discovered in the evolution of miniTurbo. The result was TurboID, with 15 total mutations relative to wild-type BirA (**Figure 1d**).

Supplementary Note 2: Discussion of mutations in TurboID and miniTurbo

Site-specific biotinylation catalyzed by wild-type BirA occurs via two half reactions: generation of the biotin-5'-AMP anhydride from biotin and ATP, followed by transfer onto a specific lysine of an acceptor peptide or protein[20]. It has been proposed that BirA-R118G (BioID) catalyzes promiscuous biotinylation by prematurely releasing biotin-5'-AMP into solution, for covalent tagging of nearby nucleophiles. **Figure 1d** shows that the 14 mutations in TurboID and miniTurbo are distributed throughout the ligase structure[16, 24], with the majority far away (>10 Å) from the bound biotin-5'-AMP. Hence, if these mutations affect biotin-5'-AMP formation rate and/or affinity, it is likely via long-range and indirect mechanisms. Previous studies have shown that wild-type BirA dimerizes upon biotin-5'-AMP formation, and disruption of this dimer decreases affinity for biotin-5'-AMP[24]. Although every mutant in our study contains an A146 deletion that decreases dimerization[17], it is possible that some of our evolved mutations further reduce dimerization; E140K, Q141R, T192A, and K194I mutations in TurboID map to the dimer interface[16,24]. In addition, removal of the N-terminal domain is known to decrease biotin-5'-AMP affinity[23]. TurboID has two mutations, Q65P and I87V, at the junction between the N-terminal domain and the catalytic core, which may alter their structural relationship, leading to reduced biotin-5'-AMP affinity.

Supplementary Note 3: TurboID and miniTurbo activities vary by cellular subcompartment

We used Western blotting to assess the activities of TurboID, miniTurbo, and BioID in the nucleus, mitochondrial matrix, ER lumen, and ER membrane of HEK 293T cells, and found that the ligase activities vary significantly in the different cellular environments (**Figure 2c**). By using the intensity of the endogenous naturally-biotinylated proteins (bands present in untransfected sample) as a reference, we can see that the signal produced by all three ligases is lower in the ER lumen and mitochondrial matrix than in the nucleus, cytosol, and ER membrane (facing cytosol). It is possible that these subcellular compartments could have chemical environments that destabilize the ligases, which could prevent efficient synthesis and release of biotin-5'-AMP. Alternatively, differences in pH and steric accessibility of proteins could change the concentration of nucleophiles (deprotonated N-termini and lysines) available for labeling.

Figure 2c also shows that the activities of TurboID and miniTurbo *relative* to BioID vary by cellular compartment. For example, in the mitochondrial matrix and ER lumen, TurboID gives stronger biotinylation in 10 minutes than BioID does in 18 hours. In the cytosol, nucleus, and ER membrane, the activity difference is not quite as pronounced. We hypothesize that, for the ER lumen, TurboID has an advantage because we evolved it in the oxidizing environment of the yeast secretory pathway. **Figure 2c** also shows that miniTurbo activity relative to TurboID is much reduced in the ER lumen and mitochondrial matrix. Removal of the N-terminal domain in miniTurbo could have destabilized the enzyme, preventing proper folding in particular chemical environments.

We also used fluorescence microscopy to assess the activities of TurboID, miniTurbo, and BioID in the mitochondrial matrix, ERM, and nucleus (**Supplementary Figures 9b; 10d, e**). The data show that in some cases, mistargeting of the ligase can occur, leading to non-specific biotinylation of proteins outside the compartment of interest. For example, **Supplementary Figures 10e** shows that BioID and TurboID fused at their N-terminal ends to a mitochondrial matrix targeting peptide give biotinylation not only in the mitochondria (expected location) but also in the cytosol and nucleus. miniTurbo does not exhibit this problem. We hypothesize that the problem arises from ligase-catalyzed biotinylation of the mitochondrial targeting peptide to which it is fused, which contains a lysine residue (MLATRVFSLVG**K**RAISTSVCVRAH). Upon biotinylation, the ability of the targeting peptide to import the ligase into the mitochondrion via the TOM/TIM pathway may be impaired, leading to ligase accumulation in the cytosol. BioID and TurboID are strongly affected, because the former requires a long biotin incubation time, and the latter can already self-biotinylate using endogenous biotin pools. Hence BioID and TurboID have ample time to biotinylate their targeting peptides, leading to accumulation of mislocalized ligase pools. This hypothesis is also supported by **Supplementary Figures 14e, f**, where mistargeting of TurboID is strongly exacerbated by long incubations with exogenous biotin (18 hours). The strong biotinylation signal in cytosol also derives from the fact that BioID and TurboID are more active in the cytosol than they are in the mitochondrion (**Figure 2c**). By contrast, miniTurbo is not affected by this phenomenon because its short labeling time (10 minutes) is not adequate to significantly alter ligase localization; although, longer incubations with biotin also do not result in significant mistargeting of miniTurbo (**Supplementary Figures 14e, f**). We suggest that the solution to this problem is to use, whenever possible, localization sequences that lack surface-exposed lysine residues that could become biotinylated by the promiscuous ligases.

Supplementary Note 4: Western blot analysis of TurboID and miniTurbo labeling specificity/radius

In addition to mass-spectrometry-based proteomics, we used Western blotting to analyze the identity of endogenous proteins enriched by TurboID and miniTurbo (**Supplementary Figure 8**). We targeted TurboID, miniTurbo, and BioID to the cytosol-facing side of the ER membrane (ERM) or to the outer mitochondrial membrane (OMM). We carried out labeling in live cells by supplementing exogenous biotin for 18 hours for BioID or 10 minutes for TurboID and miniTurbo, lysed the cells, and enriched the biotinylated proteins using streptavidin beads. We then eluted the biotinylated proteins from the beads and blotted the eluate for various endogenous ER and mitochondrial markers (**Supplementary Figure 8d**). The blots show that the endogenous ERM protein BCAP31 is enriched by ERM-ligases but not by OMM-ligases; and that endogenous

OMM proteins Tom70, Tom20, and HXK I are preferentially enriched by OMM-ligases over ERM-ligases. NDUFS6 (mitochondrial matrix protein) and calreticulin (ER lumen protein), which are not accessible to the ligases or biotin-5'-AMP generated by the ligases, are not enriched. The preferential enrichment of accessible proteins proximal to the ligases suggest that they have labeling radii on the order of a few nanometers. Note that in these experiments, OMM-miniTurbo expression level was very low, explaining the absence of enrichment. Imaging of cells expressing the ERM and OMM-targeted ligases also show that the biotin signal is proximal to the organelle expressing the ligase, again supporting short labeling radius (**Supplementary Figure 8e**).

Our ERM proteomic experiment showed that the specificity of TurboID labeling decreases with longer labeling times, suggesting that its labeling radius increases when biotin is supplied for long periods of time (likely due to saturation of proximal labeling sites, allowing the reactive biotin-5'-AMP to travel farther and tag distal proteins). Although biotinylation is greatly increased upon addition of exogenous biotin for any period of time, **Figures 2a-c** and **Supplementary Figures 6-7** show that TurboID can catalyze some biotinylation in HEK 293T cells over the 18-36 hours that it has access to the low levels of biotin present in culture media. Therefore, we wondered how this incubation with low concentrations of biotin for long periods of time affects the labeling radius of TurboID. To address this, we used our ERM proteomic data to determine which proteins are biotinylated by TurboID prior to addition of exogenous biotin. Comparing protein enrichment between our ERM-TurboID (no biotin) sample and our untransfected sample, we find that most proteins biotinylated by ERM-TurboID prior to exogenous biotin addition are indeed ER-associated secretory proteins (**Supplementary Figure 11**). Hence, this "pre-labeling" by TurboID on the ER membrane does not appear to diminish the specificity or labeling radius of TurboID.

Supplementary Note 5: Testing miniTurbo and TurboID toxicity in flies, cell culture, and worms

In flies, we performed morphological and survival assays to check for possible toxic effects of BioID, TurboID, or miniTurbo expression. Animals expressing these transgenes in the larval wing disc using *ptc-Gal4*, with or without biotin supplementation, gave rise to adult flies with no obvious defects in wing morphology (data not shown). Since *ptc-Gal4* expresses in only a subset of the wing disc, we repeated these experiments using *nub-Gal4*, which expresses in all wing disc cells that give rise to the blade of the adult wing. As with *ptc-Gal4*, we found no change in adult wing morphology or size (**Supplementary Figure 13a-c)**. When expressed ubiquitously using *Act-Gal4*, BioID and miniTurbo were non-toxic, but TurboID flies showed decreased survival and were smaller in size when grown without biotin supplementation (**Supplementary Figure 13d, e)**. We hypothesize that TurboID, which appears to have a lower K_M for biotin than BioID and miniTurbo, can consume significant amounts of the available free biotin and effectively biotin starves cells when expressed ubiquitously. In support of this, toxicity can be rescued by supplementing the fly's food with exogenous biotin. In contrast to ubiquitous expression, we find no evidence of toxicity of TurboID without biotin supplementation using a panel of Gal4 drivers that each expresses in major tissue types (i.e. muscle, neuron, glia, fat, gut, blood cells, and liver-like oenocytes) (**Supplementary Figure 13f)**.

To test for possible toxicity of TurboID, miniTurbo, and BioID expression in mammalian cell culture, we assayed cell growth in the absence versus presence of ligase expression in the cytosol or mitochondrial matrix of HEK293T cells. Because the mitochondria contains biotin-dependent carboxylases, it is an organelle that could be particularly sensitive to biotin starvation. Perturbation of mitochondrial health caused by the presence of ligase could result in slowed cellular growth, or perturbation of mitochondrial morphology. Therefore, in addition to assaying cell growth, we also assessed mitochondrial morphology in cells expressing the ligases in the mitochondrial matrix by immunofluorescence microscopy. **Supplementary Figures 14a-d** show that there is little difference in growth over 4 days, when HEK293T cells express these ligases in either compartment and exogenous biotin is not supplied. We also did not see perturbation of mitochondrial morphology when any of the ligases are targeted to the mitochondrial matrix in the absence (or presence) of exogenous biotin (**Supplementary Figures 14e, f**). In contrast to our *in vivo* observations, ordinary growth media may contain sufficient quantities of biotin such that a small amount of usage by TurboID does not influence the cell's overall biotin supply.

We do, however, observe a growth defect when TurboID or miniTurbo are incubated with exogenous biotin for 1 day or more (**Supplementary Figures 14a-d**), a far longer incubation than our recommended labeling time of 10 minutes. We hypothesize that this growth defect could be due to the high activity of TurboID and miniTurbo, whose long-term promiscuous biotinylation of endogenous proteomes is detrimental to the cell. Note that in our *in vivo* experiments, the TurboID and miniTurbo expression levels are far lower, and exogenous biotin incubation for days does not seem to have a toxic effect (**Figures 3c-g, Supplementary Figures 12b, d, Supplementary Figure 13**). Hence, users of this method should carefully consider TurboID/miniTurbo expression levels and labeling time periods when designing their experiments, in order to avoid possible toxicity from either biotin starvation or excessive promiscuous biotinylation of endogenous proteomes.

To explore the possibility of BioID or TurboID toxicity in worms, we compared the viability and developmental timing of worms expressing BioID or TurboID in the intestine. We performed viability assays and took note of any developmental delays (**Supplementary figure 16**). We measured percent viability and percent developmental delay of worms expressing BioID or TurboID in the intestine or their sibling array negative worms (control) in either biotin+ or biotin- conditions. Intestinal expression of BioID or TurboID did not considerably affect viability in either biotin+ or biotin- conditions. However, expression of TurboID slightly delayed developmental timing of worms in both biotin+ and biotin- conditions. We hypothesize that, like

in cell culture, extensive biotinylation of the endogenous proteome by TurboID throughout the 3-day period from embryo to adult may affect the developmental timing of worms that express the ligase at high concentrations.

References

1. Howarth, M. & Ting, A. Y. Imaging proteins in live mammalian cells with biotin ligase and monovalent streptavidin. *Nat. Protoc.* **3,** 534–545 (2008).

2. Bobrow, M. N., Harris, T. D., Shaughnessy, K. J. & Litt, G. J. Catalyzed reporter deposition, a novel method of signal amplification application to immunoassays. *J. Immunol. Methods* **125,** 279–285 (1989).

3. Gene Ontology Consortium. Gene Ontology Consortium: going forward. *Nucleic Acids Res.* **43,** D1049-56 (2015).

4. Ashburner, M. *et al.* Gene Ontology: tool for the unification of biology. *Nat. Genet.* **25,** 25–29 (2000).

5. Hung, V. *et al.* Proteomic mapping of cytosol-facing outer mitochondrial and ER membranes in living human cells by proximity biotinylation. *eLife* **6,** (2017).

6. Rhee, H.-W. *et al.* Proteomic Mapping of Mitochondria in Living Cells via Spatially Restricted Enzymatic Tagging. *Science* **339,** 1328–1331 (2013).

7. Thul, P. J. *et al.* A subcellular map of the human proteome. *Science (80-.).* **356,** eaal3321 (2017).

8. Muthusamy, B. *et al.* Plasma proteome database as a resource for proteomics research. *Proteomics* **5,** 3531–3536 (2005).

9. Pagliarini, D. J. *et al.* A Mitochondrial Protein Compendium Elucidates Complex I Disease Biology. *Cell* **134,** 112–123 (2008).

10. Wen, W., Meinkotht, J. L., Tsien, R. Y. & Taylor, S. S. Identification of a signal for rapid export of proteins from the nucleus. *Cell* **82,** 463–473 (1995).

11. Kalderon, D., Roberts, B. L., Richardson, W. D. & Smith, A. E. A short amino acid sequence able to specify nuclear location. *Cell* **39,** 499–509 (1984).

12. Perocchi, F. *et al.* MICU1 encodes a mitochondrial EF hand protein required for Ca2+ uptake. *Nature* **467,** 291–296 (2010).

13. Snapp, E. L. *et al.* Formation of stacked ER cisternae by low affinity protein interactions. *J. Cell Biol.* **163,** 257–269 (2003).

14. Gomord, V. *et al.* The C-terminal HDEL sequence is sufficient for retention of secretory proteins in the endoplasmic reticulum (ER) but promotes vacuolar targeting of proteins that escape the ER. *Plant J.* **11,** 313–325 (1997).

15. Seth, R. B., Sun, L., Ea, C.-K. & Chen, Z. J. Identification and characterization of MAVS, a mitochondrial antiviral signaling protein that activates NF-kappaB and IRF 3. *Cell* **122,** 669–682 (2005).

16. Wood, Z. A., Weaver, L. H., Brown, P. H., Beckett, D. & Matthews, B. W. Co-repressor induced order and biotin repressor dimerization: A case for divergent followed by convergent evolution. *J. Mol. Biol.* **357,** 509–523 (2006).

17. Weaver, L. H., Kwon, K., Beckett, D. & Matthews, B. W. Corepressor-induced organization and assembly of the biotin repressor: a model for allosteric activation of a transcriptional regulator. *Proc. Natl. Acad. Sci. U. S. A.* **98,** 6045–50 (2001).

18. Wilson, K. P., Shewchuk, L. M., Brennan, R. G., Otsuka, A. J. & Matthews, B. W. Escherichia coli biotin holoenzyme synthetase/bio repressor crystal structure delineates the biotin- and DNA-binding domains. *Proc. Natl. Acad. Sci. U. S. A.* **89,** 9257–61 (1992).

19. Eginton, C., Naganathan, S. & Beckett, D. Sequence-function relationships in folding upon binding. *Protein Sci.* **24,** 200–211 (2015).

20. Choi-Rhee, E., Schulman, H. & Cronan, J. E. Promiscuous protein biotinylation by Escherichia coli biotin protein ligase. *Protein Sci.* **13,** 3043–50 (2004).

21. Roux, K. J., Kim, D. I., Raida, M. & Burke, B. A promiscuous biotin ligase fusion protein identifies proximal and interacting proteins in mammalian cells. *J. Cell Biol.* **196,** 801–810 (2012).

22. Kwon, K. & Beckett, D. Function of a conserved sequence motif in biotin holoenzyme synthetases. *Protein Sci.* **9,** 1530–1539 (2000).

23. Xu, Y. & Beckett, D. Evidence for interdomain interaction in the Escherichia coli repressor of biotin biosynthesis from studies of an N-terminal domain deletion mutant. *Biochemistry* **35,** 1783–1792 (1996).

24. Eginton, C., Cressman, W. J., Bachas, S., Wade, H. & Beckett, D. Allosteric coupling via distant disorder-to-order transitions. *J. Mol. Biol.* **427,** 1695–1704 (2014).